DETECTABILITY OF FOREST RAINFALL INTERCEPTION THROUGH GNSS SIGNAL MEASUREMENT WITH LOW-COST RECEIVER

CHRISTIAN SARUNGALLO
September, 2022

SUPERVISORS:

Dr.-ing. Roelof Rietbroek, ITC
Dr. ir. Christiaan Van der Tol, ITC

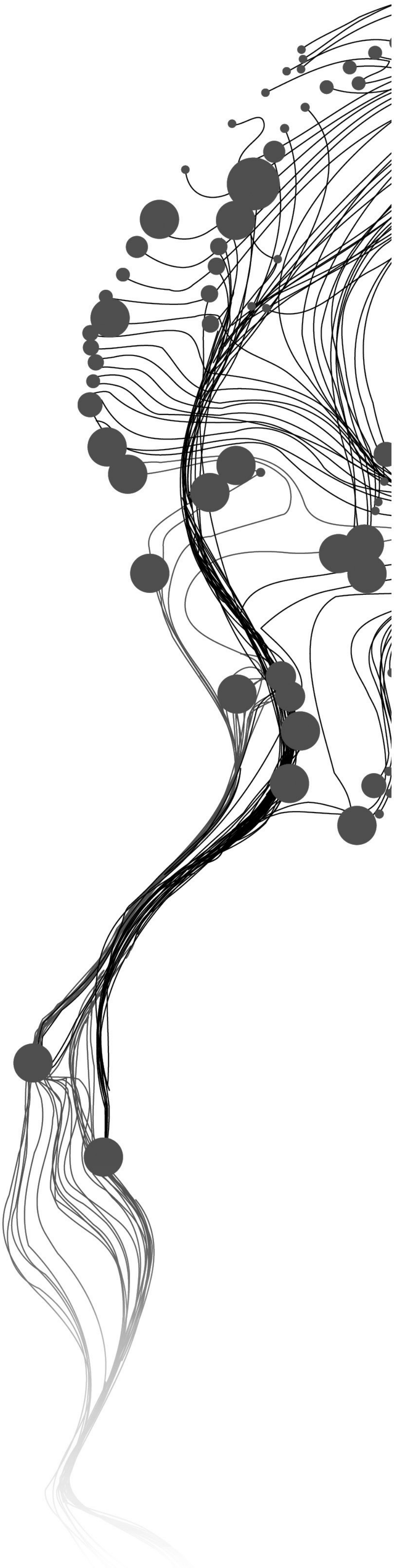

DETECTABILITY OF FOREST RAINFALL INTERCEPTION THROUGH GNSS SIGNAL MEASUREMENT WITH LOW-COST RECEIVER

CHRISTIAN SARUNGALLO
Enschede, The Netherlands, September, 2022

Thesis submitted to the Faculty of Geo-information Science and Earth Observation of the University of Twente in partial fulfilment of the requirements for the degree of Master of Science in Geo-information Science and Earth Observation.
Specialization: WREM

SUPERVISORS:

Dr.-ing. Roelof Rietbroek, ITC
Dr. ir. Christiaan Van der Tol, ITC

THESIS ASSESSMENT BOARD:

Dr. ir. R. Van Der Velde, ITC (chair)
Dr. Makan Karegar, University of Bonn (External examiner)

ABSTRACT

Forest rainfall Interception is the portion of the gross rainfall that does not reach the soil due to the leaves and branches of the tree. It is one of the important aspects related to hydrology. It influences the climate system through its role in the hydrological cycle. Forest rainfall interception influences the amount of infiltration on the forest floor, sub-surface run-off, soil moisture as well as flood generation. This study attempts to detect forest rainfall interception using GNSS measurement with a low-cost antenna. The global National Satellite System (GNSS) is a constellation of satellites for timing and positioning. The signals from GNSS are influenced (degraded) by the nearby surface of an object and can be recorded as Signal to Noise ratio (SNR) using a low-cost GNSS antenna. SNR from GNSS is such undervalued information as the signals that travel through the atmosphere and forest will degrade the GNSS signal which is commonly discarded for positioning purposes. However, the SNR information has been successfully used to derive geophysical information such as snow depth, soil moisture, wind speed etc. The attenuation of the GNSS signals due to forest has been analysed by Liu et al. (2017) to predict attributes such as biomass, and diameter at the breast height (DBH) of the forest. This opens up an idea to analyse the effect of GNSS signal attenuation due to rainfall interception. Forest rainfall interception in this study was estimated using a physical-based model by Gash, Lloyd, and Lachaud (1995). The low-cost GNSS antenna receiver was installed under the canopy that continuously received the signals transmitted by GNSS satellites. The signals recorded in SNR were correlated to the forest rainfall interception that has been estimated using Gash et al. (1995) model in an attempt to test the ability to detect interception with a low-cost antenna. The SNR data was represented in two metrics from each pass of a single satellite which are the mean value and intercept value of quadratic polynomial of SNR data. This was performed in two different scenarios based on the azimuth angle of 0-120°and elevation angle of 20-70°for scenario I and it was a 60-90°azimuth angle and 40-60°elevation angle for scenario II. It was hypothesized that SNR data will have a negative/reverse correlation with forest rainfall interception as the presence of water will attenuate/degrade the signals. However, the metrics extracted from these two scenarios established in this study did not give a significant correlation when they were plotted against forest rainfall interception. Some of the challenges and limitations were highlighted that might influence this current study. these issues are the lack of in-situ measurements for meteorological data and the latest data for forest parameters, and the impact of atmospheric attenuation remains unknown. Hence, for future study, these issues should be solved or minimized.

Keywords

GNSS, SNR, Forest rainfall Interception

ACKNOWLEDGEMENTS

To my supervisor Dr.-ing. Roelof Rietbroek, my sincere thanks for your invaluable assistance, guidance and patience leading to the completion of this Msc thesis and also to my second supervisor Dr. ir. Christiaan Van der Tol and my assesor Dr. ir. R. Van Der Velde. I later discovered that I knew nothing about this topic and decided to pursue it nevertheless out of pure curiosity. Even though I had a difficult time working on this topic, I still remember some good times building the antenna under your guidance and installing it in the Speulderbos. I am forever grateful for my time working with you.

To Wulan, Philipp, Roelant, Jonathan, Mr Olivier and Mr Schube, thanks for your generosity and support during my study. To Nick, I really appreciate all your help, support and time including helping me with my python code all the way from New York. I won't be reaching the finish line without all of you. To Ruud, thanks for everything, your outlook and advice encourage me to remain composed, and optimistic during my awful day.

I would also like to thank all my friends at Geo-information and Earth Observation (ITC) faculty, my fellow Indonesians Maulia, Tsaqif and Dewi, my fellow classmates and our mentor Arno in Water Resources and Environmental Management specialisation.

To all my siblings and cousins Aflin, Gideon, Francisco, Robinson, Gabriel, and both na honja a.k.a Omega and Ani. Thanks for all of your love and support. A special thanks to my parents whom I will always be indebted. I am everything I am because of you. Thanks for all of your love and compassion.

Above all, Kurre sumanga' Puang tu panganta'mi na mangka marampa' tu mintuna' lalan sia sara' ku olai untuntun kamanarangan in de' tana Balanda.

Christian
Amsterdam, Netherlands
14th of September 2022

TABLE OF CONTENTS

Abstract i

Acknowledgements ii

1 Introduction 1

1.1 The importance of Capturing Rainfall Interception 1

1.2 Signal to noise ratio as an undervalued source of information 2

1.3 The advancement in GNSS Reflectometry 3

1.4 The Challenge of Forest Canopy Sensing 4

1.5 Contribution of This Study 5

1.6 Objectives and Research Questions 5

1.7 Thesis Structure 6

2 Interaction of The Forest Canopy With The Surface 8

2.1 The Importance of Forest Canopy and Its Interaction 8

2.2 Forest Rainfall Interception 9

3 Sensitivity of GNSS Observations to Forest Observable 11

3.1 Principle of GNSS 11

3.2 GNSS Signals 12

3.2.1 GNSS Positioning Measurement 14

3.3 GNSS Signal Strength Information 16

3.3.1 GNSS signal Scattered and attenuated by the Forest Canopy 17

3.3.2 Multipath Effect 19

3.3.3 Signals to Noise Ratio (SNR) for GNSS-Reflectometry 20

3.4 Carrier to Noise Signal as an Undervalued Source of Geophysical Information . 21

4 Study Area, Data & Methodology 23

4.1 Study Area 23

4.2 Datasets & Instruments 23

4.2.1 Dataset 23

4.2.2 Instrument 25

4.3 Methodology 26

4.3.1 Instrument preparation and installation 26

4.3.2 SNR data processing 28

4.3.3 Extracting Metrics for SNR 30

4.3.4 Rainfall interception by forest canopy 33

4.3.5 Observe the correlation between rainfall interception and SNR 35

5 Results 36

5.1 Interception loss Estimation 36

5.1.1 Meteorological and forest Parameter 36

5.1.2 Comparison between measured and estimated Interception loss 38

5.2 Matching the temporal resolution of Meteorological data and Signal to Noise Ratio (SNR) metrics data 38

5.3 Relationship between Interception loss and SNR Metrics from GNSS measurement 40

5.3.1 Scenario I (azimuth 0-120°and elevation angle 20-70°) 40

5.3.2 Scenario II (azimuth 60-90°and elevation angle 40-60°) 44

6 Conclusions & Discussion 46

7 Recommendation 50

A Other figures 51

A.1 SNR data >30 minutes of a single pass of a satellite on Scenario I 51

A.1.1 Logarithmic Scale (dB-Hz) 51
A.1.2 Linear Scale (Volt/Volt) 52
A.2 SNR data >30 minutes of a single pass of a satellite on Scenario II 52
A.2.1 Logarithmic Scale (dB-Hz) 52
A.2.2 Linear Scale (Volt/Volt) 53

List of References **54**

LIST OF FIGURES

1.1 GNSS signals received by the ground-based antenna which consist of direct signals, reflected signals and scattered and attenuated signals that penetrate through forest canopy 2

1.2 The upper picture shows the SNR of a single satellite as the function of elevation angle. It contains direct signals and reflected signals from the planar reflector hence, we can still see the oscillation compared to the lower picture which shows SNR data from the antenna installed under the canopy due to reflected signals coming from everywhere (tree leaves, branches and might also be from the forest floor(modified from Chang et al. (2019)) 4

3.1 The triangulation principle (https://www.x.bike/blog/gps-location-and-geofence) 12

3.2 Orbital of the 24-satellite constellation for 1 July 1993 in 2D (Peter J.G. Teunissen & Oliver Montenbruck, 2017) 13

3.3 Sky plot shows the GPS satellites' traces over the Speulderbos, Netherlands over the period of 24 hours in 26_{th} of June 2022. Due to the orbital plane of the GPS satellite, no satellite trace on the northern part of the sky (gnssmissionplanning.com/App/Skyplot) 13

3.4 Code measurements (Warner & Johnston, 2003) 14

3.5 Pseudorange Model (Takasu, 2013) 15

3.6 Principle of Carrier Phase Measurement (Perez-Ruiz & K., 2012) 16

3.7 The signal received by the antenna under the forest canopy 17

3.8 The phasor diagram illustrates the carrier tracking loop on the received GNSS signal under direct and multipath effect or reflected signals. The quadrature and in-phase components of the signal are specified in Q and I axes respectively. There are three phasor indicated as A_{d}, A_{m}, and A_{c} which are amplitudes of the direct, multipath and the composite of signals respectively.ϕ_{d}, ϕ_{c}, $\delta\phi$ respectively are phase of direct, composite signals and the phase error due to multipath. The relative phase of multipath is specified as ψ which is relative to direct amplitude (Larson et al., 2008) 20

3.9 Geometry model of GNSS reflectometry in the case of a planar reflector. h is the height of the antenna concerning the planar reflector and θ is the elevation angle (Farzaneh, Parvazi, & Shali, 2021) 21

4.1 Study area in Speulderbos: (a) Location map in the Netherlands; (b) Speulderbos satellite view (c) a 47.4m scaffolding tower; (d) top view of the canopy. 24

4.2 GSV phrase for GPS 24

4.3 (a) Raspberry pi; (b) GPS hat module; (c) low-cost mass-market GPS L1 antenna; (d) Instrument combination (Captured by : Christian Sarungallo) 28

4.4 Methodology workflow 29

4.5 (a) Fresnel zones in mapview for GNSS site Speulderbos. Elevation angles are 5,10 and 15 which are indicated in green, cyan and blue respectively. An HR value of 11 m was used; (b) Screenshot of first Fresnel zones for GNSS site Speulderbos with the reflection zone for elevation angle of 5,10 and 15 projected on a Google Earth image. An HR of 11 was used as well (created using Matlab codes by Roesler and Larson (2018)) 30

4.6 GNSS antenna Installed on the tower 11 m above the ground 30

4.7 Area of interest based on the azimuth of Scenario I 31

4.8 GNSS Signals Received by the antenna under the forest canopy. The signal from the satellite (a) with the high elevation angle (θa) travels a shorter part of the forest canopy compared to satellite (b) with the low elevation angle (θb) hence, mostly the signals from low elevation angle will be scattered and attenuated. H is antenna height from the ground and T is canopy thickness. 31

4.9 Area of interest based on the azimuth of Scenario II 32

4.10 (a) SNR data with respect to elevation angle in (dB Hz) and (b) in linear scale (volt/volt) 33

4.11 (a) SNR metric which shows mean of SNR for a single pass of satellite and (b) quadratic polynomial plotting to extract constant value as the metric of SNR for a single pass of a satellite 33

5.1 Monthly rainfall and interception from the average value of 3 different stations (Lelystad, De Bilt, and Deelen) during the study 37

5.2 (a). The hypothesis of the relationship between SNR value to interception loss (b). SNR, where mean, is used as a metric (dB-Hz) with respect to interception loss (mm) (c). SNR, where intercept from quadratic polynomial, is used as a metric (dB-Hz) with respect to interception loss (mm) 41

5.3 (Scenario I) Forest condition with respect to the median from SNR Metrics (dB-Hz) 42

5.4 (a). SNR, where mean, is used as a metric (Volt/Volt) with respect to Interception loss (mm) (b). SNR, where intercept from quadratic polynomial, is used as a metric (Volt/volt) with respect to interception loss (mm) 42

5.5 (Scenario I)Forest condition with respect to the median from SNR metrics (Volt/Volt) 43

5.6 (a). SNR, where mean, is used as a metric (dB-Hz) with respect to interception loss (mm) (b). SNR, where intercept from quadratic polynomial, is used as a metric (dB-Hz) with respect to interception loss (mm) 44

5.7 (a). SNR, where mean, is used as a metric (Volt/Volt) with respect to interception loss (mm) (b). SNR, where intercept from quadratic polynomial, is used as a metric (Volt/volt) with respect to interception loss (mm) 45

6.1 SNR data from a single pass of the satellite with respect to sin elevation angle . . 49

A.1 (a). SNR, where mean, is used as a metric (dB-Hz) with respect to interception loss (mm) (b). SNR, where intercept from quadratic polynomial, is used as a metric (dB-Hz) with respect to interception loss (mm) 51

A.2 (a). SNR, where mean, is used as a metric (dB-Hz) with respect to interception loss (mm) (b). SNR, where intercept from quadratic polynomial, is used as a metric (dB-Hz) with respect to interception loss (mm) 52

A.3 (a). SNR, where mean, is used as a metric (dB-Hz) with respect to interception loss (mm) (b). SNR, where intercept from quadratic polynomial, is used as a metric (dB-Hz) with respect to interception loss (mm) 52

A.4 (a). SNR, where mean, is used as a metric (dB-Hz) with respect to interception loss (mm) (b). SNR, where intercept from quadratic polynomial, is used as a metric (dB-Hz) with respect to Interception loss (mm) 53

LIST OF TABLES

4.1 The description of GSV phrase based on the figure 4.2 (https://cdn-shop.adafruit.com/product-files/5186/5186_PA1616D_Datasheet.pdf) 25

4.2 The description of NMEA output sentences (https://cdn-shop.adafruit.com/product-files/5186/5186_PA1616D_Datasheet.pdf) 26

4.3 The description of the CD-PA1616D GNSS patch antenna module (https://cdn-shop.adafruit.com/product-files/5186/5186_PA1616D_Datasheet.pdf) 27

5.1 The forest state parameter values of canopy storage derived from Cisneros Vaca, Van Der Tol, and Ghimire (2018) and fraction vegetation cover of the coniferous forest at the Veluwe area by Hahirwabasenga (2019) 36

5.2 The summary of meteorological parameters and interception loss estimation in this study 37

5.3 Monthly rainfall and interception loss in the period of 26 March to 26 June . . . 37

5.4 Measured Interception loss and mean evaporation (Cisneros Vaca, Van Der Tol, & Ghimire, 2018) 38

5.5 (Scenario I) Meteorological parameters and interception loss estimation after the temporal resolution has been matched with SNR data 39

5.6 (Scenario I) Meteorological parameters and interception loss estimation after the temporal resolution has matched with SNR data 39

5.7 (Scenario I (dB-Hz)) median and mean value of SNR metrics based on the forest condition 41

5.8 (Scenario I (Volt/Volt)) median and mean value of SNR metrics based on the forest condition 42

6.1 The summary of interception loss for Douglas-fir forest, [a] Mixed Douglas-fir and Western hemlock. This table is adapted from Cisneros Vaca, Van Der Tol, and Ghimire (2018) 47

Chapter 1

Introduction

1.1 THE IMPORTANCE OF CAPTURING RAINFALL INTERCEPTION

Rainfall interception is the amount of rainfall intercepted by the forest and evaporates back into the atmosphere. The amount of rainfall that does not manage to reach the soil is quantified as the interception loss (mm). The interception loss based on I. R. Calder (1990) in the upland catchments of Britain accounts for 35% with annual rainfall $>$ 1000mm and about 40-50% in the area where the rainfall is around 500-600 mm. However, interception loss does not depend only on the intensity of rainfall but it depends also on vegetation type, structure and cover of the forest and potential of evaporation (Carlyle-Moses & Price, 2007; Chow, 1959; Dunne & Leopold, 1978; V. Jetten, 1996; Llorens & Domingo, 2007). Based on the study conducted by Cisneros Vaca, Van Der Tol, and Ghimire (2018), the interception loss (mm) accounts for 38% of gross rainfall in a mature Douglas fir stand in the Netherlands.

Based on the proportion of forest interception on rainfall, the interception loss can not be disregarded from hydrological models. Through hydrological cycle interception influences, the climate system and the recycling of the local rainfall (Bonan, 2008; Rotenberg & Yakir, 2010). In the hydrological cycle, interception is the first chain from rainfall to run-off which influences infiltration (soil moisture). Some models have developed due to the significance of rainfall interception. Amongst the models that have been developed, the physical-based models have been considered the most for the Interception study (Muzylo et al., 2009). These physical models are the analytical model of rainfall (Gash et al., 1995) and storm-based analytical (Gash, 1979). Both the models are further explained in the next chapter under the section 2.2 for the need of this study.

Most of the interception loss studies were conducted at the plot level of trees where throughfall which is the portion of rainfall that can reach the forest floor is measured (David et al., 2006; Gash & Morton, 1978; Ghimire, Bruijnzeel, Lubczynski, & Bonell, 2012; Mateos & Schnabel, 2001; Pereira et al., 2009). From the measurements of the throughfall where the fractions of interception loss are derived (Aston, 1979; Bryant, Bhat, & Jacobs, 2005; Ian R Calder, 2001; Gómez, Giráldez, & Fereres, 2001; Victor Gerlof Jetten et al., 1994; Pypker, Bond, Link, Marks, & Unsworth, 2005). At the large-scale level, it would be difficult to implement these studies. Therefore, to provide the solution for interception loss estimation, new techniques such as GNSS signal measurement are worth investigating.

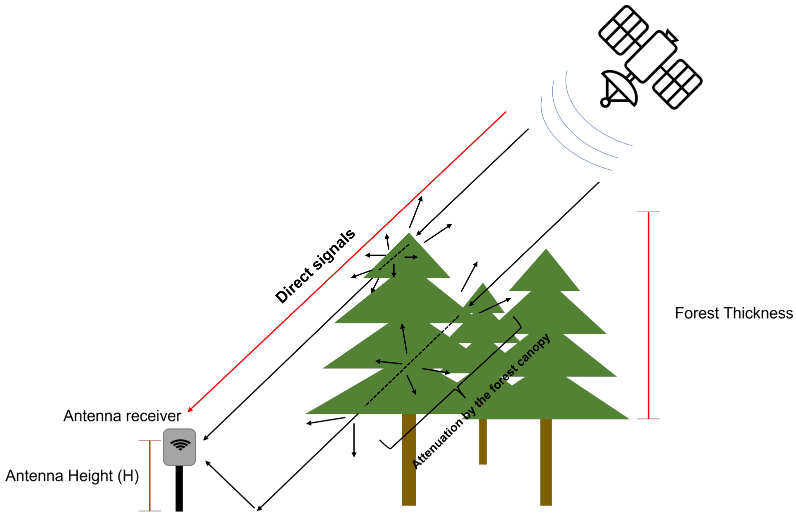

Figure 1.1: *GNSS signals received by the ground-based antenna which consist of direct signals, reflected signals and scattered and attenuated signals that penetrate through forest canopy*

1.2 SIGNAL TO NOISE RATIO AS AN UNDERVALUED SOURCE OF INFORMATION

The Global Navigation Satellite System (GNSS) is a constellation of satellites that transmit signals for positioning and timing data to a ground-based receiver. GNSS signals are degraded negatively by the signals reflected by the nearby surface of an object. Figure 1.1 illustrates the signals received by the antenna installed under the canopy. The antenna does not only receive direct signals but also signals that have been scattered and attenuated by the forest or might be some of the reflected signals from the forest floor. The reflected signals travel a longer path compared to direct signals before arriving at the antenna. The reflected signals and those signals that have been scattered and attenuated will interfere with direct signals known as multipath.

The multipath can be visible in the Signals to Noise Ratio (SNR). For positioning purposes, the multipath effect causes noise which needs to be mitigated. This can be done by rejecting low elevation signals, using a geodetic antenna which is less sensitive to reflection and left-hand circular polarized (LHCP) signals and using SNR for outlier detection and weighing in position algorithms. However, GNSS Reflectometry takes advantage of this as the source of valuable information such as geophysical characteristics of the earth's surface properties such as sea level (Lowe et al., 2002; Martin-Neira, 1993), sea ice thickness (Komjathy, Maslanik, Zavorotny, Axelrad, & Katzberg, 2000) land surface conditions, including snow depth (Cardellach, Fabra, Rius, Pettinato, & D'Addio, 2012; Rodriguez-Alvarez, Camps, et al., 2011), soil moisture (Masters, 2004).

Furthermore, GNSS signal strength which is measured in SNR can be used to predict forest attributes such as diameter at breast height, tree height and stem volume (Liu et al., 2017). The signal penetrates through the forest canopy is analysed to see how the attenuation by the forest canopy impacts the SNR. Besides, Rodriguez-Alvarez et al. (2012) tried to retrieve vegetation water content by observing the attenuation power of GNSS signals. This study has enabled the first approximation to infer a factor related to leaves and opacity of the forest and it shows good agreement of the GNSS measurement and ground truth data of a factor related to leaves ($r = 93\%$).

1.3 THE ADVANCEMENT IN GNSS REFLECTOMETRY

GNSS multipath signals have been exploited opportunistically to retrieve land surface characteristics such as soil moisture, snow depth, and vegetation changes. These versatility results can be the source of opportunities to implement GNSS reflectometry as a promising remote sensing technique (Jin, Cardellach, & Xie, 2014; Zavorotny, Gleason, Cardellach, & Camps, 2014).

Wind Speed

Komjathy et al. (2004), found that the estimated wind speed produced from surface-reflected GPS data shows good agreement (within 2 m/s) with data from a nearby buoy and independent wind speed measurements taken from the TOPEX/Poseidon altimetric satellite. This was done by collecting the measurement of GNSS reflected signals using aircraft with a delay mapping receiver during flights to the Hurricanes Michael and Keith in October 2002.

Soil Moisture

In the study conducted by Larson et al. (2009) on soil moisture, over 7 months from the continuously operating geodetic quality GPS receiver in the U.S. that manage by Planet Boundary Observatory (PBO), National Science Foundation (NSF) and National Geodetic Survey (NGS). The soil moisture measurements from conventional water content reflectometer sensors (in-situ measurement) demonstrate good agreement ($r^2 = 0.9$ to 0.76) with the variation in the frequency of reflected GPS signals, with the majority of the disagreement occurring when the soil moisture content is less than 0.1 cm^3/cm^3.

Snow Depth

For the study on snow depth, McCreight, Small, and Larson (2014), discovered that the mean snow depth measured manually at 18 sites in the Rocky Mountains, in the U.S., in the 1000 m^2 scale region around each antenna is reasonably similar to the daily snow depth determined from GPS reflection data. This comparison covers depths ranging from 0 to 150 cm on average across the site. Across this range of snow depths, the GPS depth data showed a minor negative bias (around -6 cm).

GNSS reflectometry has become one of the alternatives for earth observation over the last two decades. The interest in GNSS signals reflected from the Earth's surface to monitor various geophysical parameters has rapidly grown. GNSS operation is regarded as highly precise, and continuous with a near real-time temporal resolution, as well as the weather condition does not bind it for the measurement since it operates in the L-band of the frequency spectrum (1-2 GHz). The signal is not very sensitive to clouds and rain hence, the impact of rain on the transmitted signals is negligible (Balasubramaniam & Ruf, 2020).

The characteristics mentioned above indicate that GNSS has huge advantages to be applied to various objects and surfaces. However, all the studies mentioned above used expensive devices e.g., geodetic-quality GNSS receivers. This antenna is designed to screen off multipath signals but for GNSS reflectometry the multipath is the source of information to be captured. The

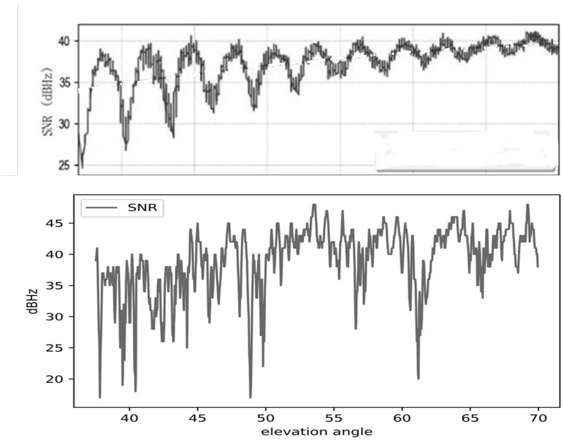

Figure 1.2: The upper picture shows the SNR of a single satellite as the function of elevation angle. It contains direct signals and reflected signals from the planar reflector hence, we can still see the oscillation compared to the lower picture which shows SNR data from the antenna installed under the canopy due to reflected signals coming from everywhere (tree leaves, branches and might also be from the forest floor(modified from Chang et al. (2019))

expensive antennas are also more sensitive to right-hand circular polarized (direct signals) compared to left-hand circular polarized signals (reflected) (Jiang & Groves, 2012). Besides, this type of antenna has a hemispherical dome shape which can not catch all the signals reflected from below the antenna. However, the low-cost antenna has disadvantages such as larger antenna phase centre errors. Low-cost antennas are also sensitive to left-hand circular polarized signals which are coming from the reflection (of Right-hand circular polarized GNSS signals) but these disadvantages re actually advantages for GNSS reflectometry.

1.4 THE CHALLENGE OF FOREST CANOPY SENSING

A few vegetation sensing studies have been done to estimate the biophysical properties and growth based on the effect of vegetation on multipath GNSS signals. Small, Larson, and Braun (2010), described a GPS multipath approach for estimating vegetation growth by using the schedule of agricultural manipulation (planting, cutting, etc.) that enabled to isolate the impact of vegetation growth on GPS multipath. Subsequently, this method can provide height and vegetation water content. In fact, according to Rodriguez-Alvarez, Bosch-Lluis, et al. (2011) the study of vegetation height retrieval showed that the mean retrieval of two different plants e.g., wheat, barley and maize agree well with ground truth data. Maize height results are quite satisfied with the Pearson correlation coefficient (ρ) and the coefficient of determination (R^2) $\sim$ 99.74%. The wheat field was shown $\rho \sim$ 89% while the coefficient of determination $R^2 \sim$ 80 and barley field with $\sim$ 97% and $R^2 \sim$ 94%.

Different from the forested area, the two studies above were carried out using GNSS reflectometry as the assumption of the planar reflector can be applied. The GNSS reflectometry is further explained in chapter 3 under the section 3.3.2 and 3.3.3. The example of the signals recorded through SNR for planar reflectors and non-planar e.g., antenna installed under the canopy can be seen in the figure 1.2.

In the forest setting Liu et al. (2017), tried predicting forest attributes by analysing the attenuation of the GNSS signals due to forest canopy. The data was collected using 2 receivers installed on an all-terrain vehicle (ATV) platform. The ATV was moving inside the forest to collect signals under the canopy called the in-forest receiver. The other receiver was placed in the open space condition called the out-forest receiver which measured the strength of signals without forest attenuation. Forest attributes, including mean canopy height, were predicted using statistical features from signals loss due to forest attenuation. The most common remotely sense forest canopy height estimations are using synthetic aperture radar (SAR) (InSAR), including polarization interferometry (PolInSAR), (Patenaude, Milne, & Dawson, 2005) which are validated by using airborne imaging light detection and ranging (LiDAR). However, the inconvenience of LiDAR is high operating cost, during heavy rain or with low-hanging clouds it is ineffective and due to the huge data sets and complexity of the data collected, data analysis may require advanced skilled techniques.

1.5 CONTRIBUTION OF THIS STUDY

The forest information retrieval through analysing GNSS signals attenuation opens up the idea to perform the same study on forest rainfall interception. This study will observe the detectability of forest rainfall interception through GNSS measurement using a low-cost antenna receiver. Similar to Liu et al. (2017), the attenuation of the GNSS signals will be analysed. It is assumed that the presence of water in the canopy will further attenuate the GNSS signals. This attenuation effect may then be observed through the SNR.

Different from Liu et al. (2017) that used two antennas in two different settings(inside the canopy and outside under the open sky) to analyse the attenuation of the GNSS signals, this study only used a low-cost antenna installed under the canopy. One of the antennas was also installed above the canopy but it was not working. The attenuation will be analysed based on the SNR of dry conditions and wet conditions. The metrics from the SNR as well as forest rainfall interception will be derived and analysed to find any correlation.

Some challenges may occur from this study such as the antenna might pick up signals from the planar reflector forest floor and atmospheric water vapour change. It will be further explained in chapter 3 regarding how significant these two effects are and whether they could be ignored. The impact of signals from the forest floor is explained under the section 3.3.1 and the impact of water vapour change is explained under the section 3.3.1.

1.6 OBJECTIVES AND RESEARCH QUESTIONS

Main Objective

The main objective of this study is to assess the capabilities of using a low-cost GNSS receiver on detecting forest rainfall interception through GNSS signals measurement. The GNSS signals will be recorded as Signal to Noise ratio (SNR) and analysed based on the dry and wet conditions of the forest.

Sub-Objectives

In an attempt to achieve the main objective, it can be further broken down into several sub-objectives as follows:

- Defining a suitable metric for forest rainfall interception from forest canopy information and meteorological data available.
- Defining metric from GNSS signals measurement from SNR data recorded by the low-cost antenna.
- Correlating the SNR from GNSS measurement to forest rainfall interception.
- Testing whether the low-cost antenna can work.

Research Question

- How to compute a representative interception estimate for the site based on the forest canopy information and meteorological data available?
- How useful are the metrics extracted from the SNR data?
- What is the correlation between forest rainfall interception and SNR data from low-cost antenna measurement?
- What are the indications or findings to conclude whether the low-cost antenna can work for this study?

1.7 THESIS STRUCTURE

The details of the study in this thesis are presented in 7 chapters and they are outlined as follows,

Chapter 1 describes the importance of the research of this thesis regarding the forest rainfall interception 1.1. This chapter also describes the SNR as the undervalued source of information 1.2, The advancement in GNSS reflectometry highlights the applicability of the GNSS-R technique 1.3. Furthermore, The challenge of the forest canopy sensing section is provided 1.4. Subsequently, the contribution of the study in this thesis 1.5, as well as the main objective and sub-objectives, are also described 1.6.

Chapter 2 is dedicated to the interaction of the forest canopy with the surface. This chapter describes the importance of the forest canopy and its interaction 2.1 which highlights the role of rainfall interception as one of the significant components of the interactions. The last section of this chapter describes how the forest rainfall interception is derived 2.2. It is important to first understand the interaction of the forest canopy, especially the role of rainfall interception as the main object of this study. This section will give insight before it is further described from the perspective of GNSS measurement in the next chapter.

Chapter 3 describes the sensitivity of GNSS observations to forest observable. This chapter is the continuation of chapter 2 but more from GNSS measurements. This chapter firstly describes the principle of GNSS 3.1and The measurement of the GNSS signal 3.2. The GNSS signal strength 3.3 which includes the impact from the attenuation due to the forest canopy, atmosphere and forest rainfall interception, is discussed in this chapter. The multipath effect 3.3.2 and SNR for GNSS-Reflectometry 3.3.3 are also provided. Subsequently, the last section is discussing the summary of SNR as an undervalued source of geophysical information 3.4.

Chapter 4 describes the Study area 4.1, the dataset and the instrument 4.2 in this study as well as the methodology 4.3 where data are being processed for forest rainfall interception and SNR data from GNSS measurement.

Chapter 5 Presents the result of all analyses conducted in this study including the estimation of forest rainfall interception 5.1 and How is the relationship between SNR and Interception loss 5.3

Chapter 6 Presents the conclusion of this study as well as a Discussion which discuss the overall findings, and limitations. The conclusion and discussion are presented by answering the research questions related to the objectives of this study

Chapter 7 Presents the potential direction and recommendation for the future study based on the discussion and elaboration of the findings as well as limitations from the previous chapter.

Chapter 2

Interaction of The Forest Canopy With The Surface

2.1 THE IMPORTANCE OF FOREST CANOPY AND ITS INTERACTION

Forest canopy is defined as "the aggregate of all crowns in a stand of vegetation" (Parker, Lowman, & Nadkarni, 1995). The canopy of a single tree consists of the crown rim and the interior of the crown. The rim includes the leaves and small twigs which is the part that gets mostly exposure to the sun. The crown interior includes the trunk and main branches which shapes the tree (Nadkarni, Merwin, & Nieder, 2013).

The forest canopy is where the primary gas exchange happens between the atmosphere and vegetation. Approximately, it is responsible for 50% of carbon exchange between the atmosphere and terrestrial ecosystem is made up by the forest canopy. The forest ecosystem is one of the key components of the global climate and terrestrial carbon cycle as it is an important carbon sink (Banskota et al., 2014). Forest serves a function as a carbon sink to reduce the build-up of CO_2 in the atmosphere which is one of the greenhouse gasses driving climate change.

The linkage between forest and climate change can be understood through the hydrological cycle. The forest canopy function as an interception for the rainfall. The forest canopy will intercept a large amount of rainfall that falls on it while some of it will reach the forest floor. In the hydrological cycle, rainfall interception is the first process in the chain from rainfall to run-off. The amount of rainfall interception will influence the infiltration on the forest floor, sub-surface runoff, soil moisture (moisture recycle) and recharge flood generation (Tsiko, Makurira, Gerrits, & Savenije, 2012).

The significant role of the forest canopy in the hydrological cycle on how it interacts with other components such as rainfall and surface run-off and infiltration (soil moisture) makes it relevant to study. Remote sensing mission through microwave signals on soil moisture retrieval showing the significant impact of the forest canopy on the signals that need to be corrected. Similar to the signal for positioning purposes from the GNSS satellite constellation, the forest canopy is also impacting this signal. This enables the study of the retrieval of forest canopy attribute through the measurement of GNSS signals. This will be further explained in the next chapter under the section 3.3.1.

The measurement of the GNSS signal related to the forest canopy opens up the opportunity to also observe the detectability of forest rainfall interception. It is assumed that the presence of water on the forest canopy will impact the GNSS signals. This case will be explained in detail in the next chapter 3.

2.2 FOREST RAINFALL INTERCEPTION

Rainfall interception refers to the part of rainfall captured by the vegetation which unable to reach the soil before it is evaporated back to the atmosphere (Cisneros Vaca et al., 2018). Rainfall interception is an essential factor to understand in the hydrological cycle as it is estimated to account for around 24-45% of gross rainfall in coniferous forest (Carlyle-Moses & Gash, 2011; Gash, Wright, & Lloyd, 1980; Rutter, Morton, & Robins, 1975).

The process of forest canopy interception is where the rainfall stays in the canopy until it evaporates back into the atmosphere generating a rainfall loss of 9% - 60% the gross rainfall in general (Ma, Li, Luo, Shao, & Jia, 2019). The interception loss (I, mm) due to the forest canopy is controlled by several factors such as the structure of the canopy (canopy storage capacity), Characteristic of the rainfall (duration, low and high intensity), the composition of the species of the vegetation, climatic condition (evaporation of the wet canopy) (Carlyle-Moses & Price, 2007; Llorens & Domingo, 2007).

There have been many physically-based models developed to estimate rainfall interception of forests. Based on the review conducted on 15 selected models of the rainfall interception by Muzylo et al. (2009), the models that were mostly used were the storm-based analytical (Gash, 1979) and analytical model of rainfall (Gash et al., 1995) (69 cases application). The storm-based analytical(Gash et al., 1995) was broadly used to estimate the rainfall interception based on the forest canopy, trunk, rainfall rate and meteorological factors. The storm-based analytical model from Gash (1979) calculates the interception by the canopy and trunk separately, hence more parameters are required such as trunk storage capacity (S_t) and stemflow (Pt) which are difficult to obtain.

The Gash model estimates rainfall interception into two conditions: low rainfall that will not saturate the canopy where gross rainfall (P_G)$<$ threshold value needed by the rainfall to saturate the canopy (P'_G). The threshold value of gross rainfall required to saturate the canopy can be given as follows:

$$P'_\mathrm{G} = -\frac{\bar{R}}{\bar{E}_\mathrm{c}} \frac{S_\mathrm{c}}{FVC} ln[1 - (\frac{\bar{E}_\mathrm{c}}{\bar{R}})] \tag{2.1}$$

The threshold value of gross rainfall that can saturate the canopy is determined only for rainfall $>$ 0.5mm/h (Gash, 1979). This value is used to define the mean rainfall rate $\bar{R}$ and the mean evaporation rate $\bar{E}_\mathrm{c}$. According to the Gash et al. (1995) these two variables were measured in the whole experimental period during the wet or saturated condition to replace the storm-based analytical model (Gash, 1979) for this study. S_c accounts for the canopy storage capacity and *FVC* is fractional vegetation cover which is the ratio of the vegetation cover of a certain area. Based on the saturation of the canopy, the rainfall interception loss (*I*) can be calculated as follows:

- Low rainfall condition that is unable to saturate the canopy ($P_\mathrm{G} < P'_\mathrm{G}$):

$$I = FVCP_\mathrm{G} \tag{2.2}$$

- High rainfall condition that can saturate the canopy ($P_\mathrm{G} > P'_\mathrm{G}$)

$$I = FVCP'_{\mathrm{G}} + (FVC\frac{\bar{E}_{\mathrm{c}}}{\bar{R}})(P_{\mathrm{G}} - P'_{\mathrm{G}}) \tag{2.3}$$

Where I is Interception loss by the canopy in (mm), $\bar{R}$ is the mean rainfall rate during the saturated condition in (mm/h), $\bar{E}_{\mathrm{c}}$ the mean evaporation rate in (mm/h), FVC is fractional vegetation cover.

Chapter 3

Sensitivity of GNSS Observations to Forest Observable

3.1 PRINCIPLE OF GNSS

In general, GNSS consists of three segments: space, ground and user segment. The space segment includes a constellation of satellites orbiting the earth in roughly circular planes (Dawoud, 2012). The ground segments which control the system are responsible for ensuring the proper operation of the satellites and also maintaining them. The user segment consists of the users e.g., civilians and military by using passive receivers that could receive signals from the satellite and decode them (Vu, 2019). GNSS military signals are not available for civilians and can only be accessed with a special receiver.

The main output from GNSS is positioning, receiver time offset and navigation. These can be estimated from the transmitted signals from the satellite constellations. To estimate position, timing, and velocity, it needs at least four satellites to get precise information. The basic concept for this estimation is called trilateration or triangulation (Jin et al., 2014). An object's distance to a satellite can be determined based on the delay in signals between these two. When the distance from a satellite to an object is known, the object can be placed around a circle centred at the satellite. The position of the object can be mathematically computed when there are known distance between an object to three different satellites based on the intersection of the three circles (figure 3.1). The atmospheric condition has an impact on the calculation of distance through delay and speed transmission(Oliveira, Zapella, & Hunt, 2018), the fourth satellite is principally needed to fix the unknown receiver clock error (time offset of the receiver). Adding more satellites will further increase the accuracy. In the case of GPS, it allows many more than 6 to 11 satellites that can be tracked depending on the location and time.

GPS Satellite Constellation

The initial goals of GPS were primarily for military purposes however, GPS service has become openly accessible for civilians as US president Ronald Reagan issued a mandate in 1983. By 1994, GPS has become fully operational as the 24th satellite was launched (Jin et al., 2014). The satellite constellations of GPS are placed nearly in a circular orbit at an altitude of 26,559km as it adopts medium-altitude Earth orbit (MEO). Launch cost and global coverage become the consideration of choosing MEO (Jin et al., 2014). The orbit of the satellites is inclined 55°with reference to the equatorial plane where four satellites are placed in each of six orbital planes. The six orbital planes are assigned with letters from A to F and at a certain epoch which are also referred to as slots.

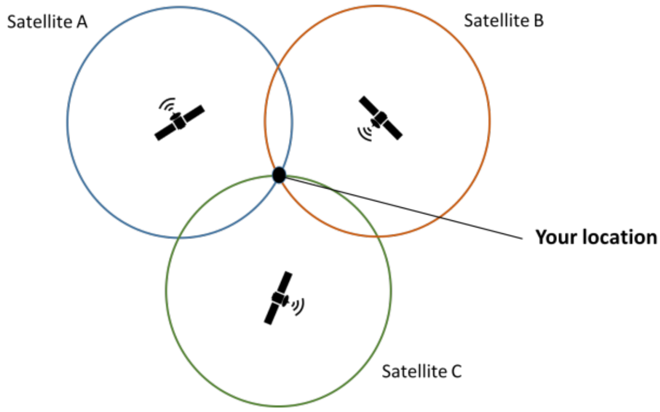

Figure 3.1: The triangulation principle (https://www.x.bike/blog/gps-location-and-geofence)

The 24 satellite locations are named based on the combination of the orbital planes' letters with numbers (figure 3.2) (Peter J.G. Teunissen & Oliver Montenbruck, 2017). It can be seen from the fig.3.2 that within the orbital plane the four slots or the position in orbit indicated by its longitude are not spaced asymmetrically. This type of design was set as the best solution against satellite failures (Beutler, Weber, Hugentobler, Rothacher, & Verdun, 1998).

The present constellation of GPS consists of up to 31 operational satellites. Some expendable slots were added to the baseline of 24 satellites. Three slots, which were B1, D2, and F2 split into two slots to make it 27 satellites in the constellation (Department Of Defense, 2008). Other beyond the 27 operational satellites are normally placed near to the satellites which are close to their replacement time (Peter J.G. Teunissen & Oliver Montenbruck, 2017)

We might think that GPS satellites cover completely all of the sky however, the satellites' visibility over the sky depends on their orbital plane. GPS satellite inclination relative to the equator is 55° hence, only for the latitudes below or equal to this inclination that can be viewed at 90° elevation (De Jong, Goode, Liu, & Stone, 2014). Besides, at all altitudes, some of the sky (at high altitudes) will not cover by the GPS satellites (Swaszek, Hartnett, Seals, Siciliano, & Swaszek, 2018). As for the example,(figure 3.3) shows traces of the GPS satellites' orbits over the Speulderbos (52.25117°N, 5.69006°E) site in the Netherlands of the period of 24 hours in 26th of June 2022 which shows no satellite in the northern sky (gap towards the north). The consequence of this gap will decrease the accuracy of positioning due to fewer satellites to no satellites visible at a certain time. in fact, the visible satellites never pass along the northern azimuths in the sky.

3.2 GNSS SIGNALS

The signal that GPS satellites transmit is an L-band signal which is similar to the signals used for microwave radar application (Small et al., 2010). These signals are transmitted at the frequency of 1575.42 MHz for link 1 (L1) and 1227.6 MHz for link 2 (L2). They are modulated by Pseudo Random Noise (PRN) ranging codes and navigation messages. There are two types of PRN used to broadcast GPS signals namely Coarse Acquisition (C/A) and code P (precise). The C/A raging code modulates L1 carrier signals while the P-code modulates both L1 and L2 carrier signals. Selective Availability (SA) and Anti-spoofing (AS) are two techniques to limit civilians from accessing the

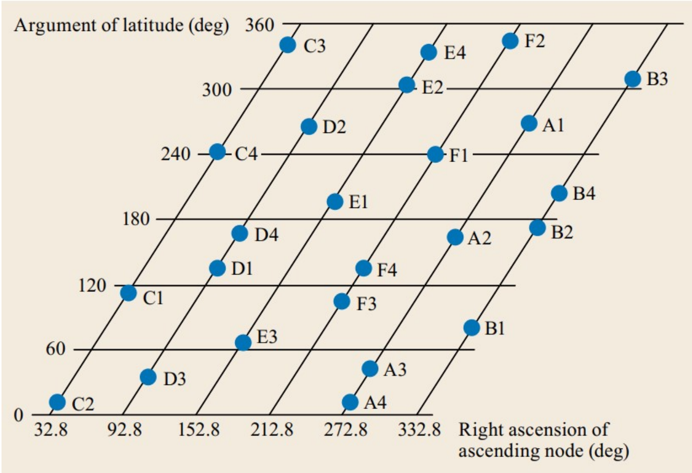

Figure 3.2: Orbital of the 24-satellite constellation for 1 July 1993 in 2D (Peter J.G. Teunissen & Oliver Montenbruck, 2017)

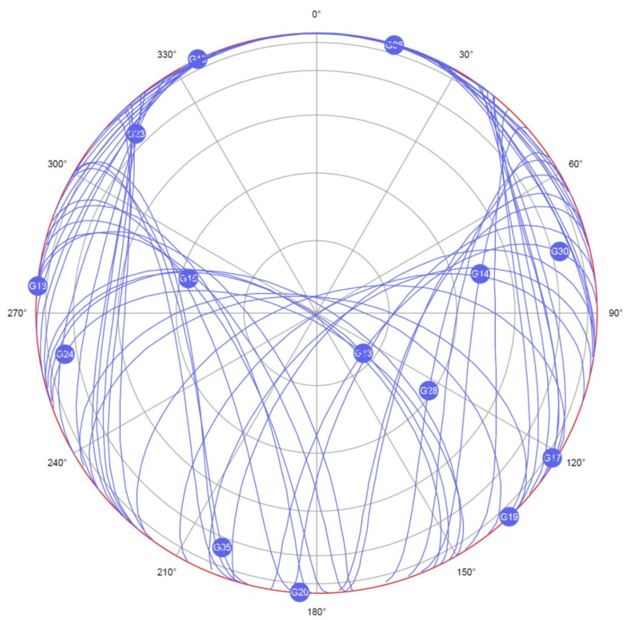

***Figure 3.3:** Sky plot shows the GPS satellites' traces over the Speulderbos, Netherlands over the period of 24 hours in 26_{th} of June 2022. Due to the orbital plane of the GPS satellite, no satellite trace on the northern part of the sky (gnssmissionplanning.com/App/Skyplot)*

full system of GPS. Selective Availability (SA) is degrading the GPS signal intentionally for C/A raging code. However, SA was eliminated in 2000 hence, C/A is unencrypted and it is open for civilian use (Hofmann-Wellenhof, Lichtenegger, & Collins, 2001). Anti-spoofing is the way to deny all access to the P-code since the P-code is only intended for military use hence, it is encrypted as a P(Y) code (Jin et al., 2014; Peter J.G. Teunissen & Oliver Montenbruck, 2017).

3.2.1 GNSS Positioning Measurement

Based on the capacities of the antenna receivers, the positioning measurements can be done in two different ways. The low-cost mass-market antennas with mono-frequency (L1) determine the position by measuring the code observations. On the other hand, the more expensive antennas with multi-frequency bands i.e., geodetic antennas use positioning based on carrier phase measurement. In terms of positioning, the carrier phase measurement is considerably more accurate (Vu, 2019). For surveying purposes, the stationary base station can improve the positioning accuracy by receiving the GNSS signals as a corrector factor which is sent to rovers.

Code Measurement

The principle of code measurement is based on one of the PRN ranging codes, which is the Coarse Acquisition (C/A) code. The C/A code consists of binary digits (0 and 1) or a sequence of 1,023 chips (bits). The C/A code has frequency of $f_0/10 = 1.023$ MHz as the fundamental frequency (f_0) of GPS is 10.23 MHz. Therefore, the sequence repetition is 1,023/(1.023MHz) = 1000 MHz^{-1} which is equals to 1 millisecond. As radio wave travels at the speed of light, 1 ms corresponds to 299.79 Km hence, each chip will equal to 293 m (Hofmann-Wellenhof et al., 2001; Hofmann-Wellenhof, Lichtenegger, & Wasle, 2008; Kaplan & Hegarty, 2006).

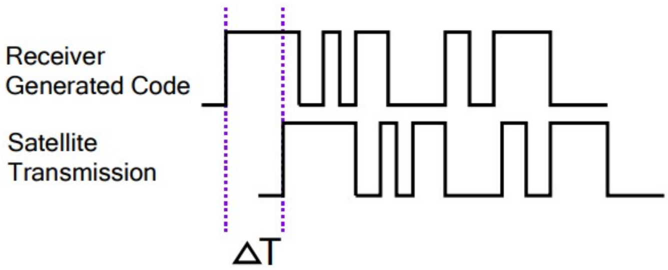

Figure 3.4: *Code measurements (Warner & Johnston, 2003)*

The GNSS receiver determines the time travel (ΔT) of the signals from the satellite by correlating the received pseudo-random code -digital code which is unique for each satellite- with a replica generated by the receiver. Travel time (ΔT) is obtained from the amount of time the receiver needs to slide its code until it syncs up with the signal from the satellite (figure 3.4). This is commonly referred to as pseudorange which is the distance between receiver and satellite which does not only include the time offset between satellite and receiver but also the biases due to the atmospheric delay, instrumental delay of receiver and satellite as well as the multipath effect. The error between the satellite and receiver clocks is obtained as offset or different time scale of the satellite (t_s) and the receiver (t_r) considering the reference time (s) (figure 3.5). Therefore pseudorange can be expressed as follows (European Space Acency, 2018):

$$R_\mathrm{p} = c(t_\mathrm{r} - t_\mathrm{s}) \tag{3.1}$$

where c is the speed of light and (t_s) and (t_r) respectively are signal transmission measured by satellite clock (s) and received signal measured by receiver clock (s). This equation can be expressed as the geometric range (ρ) between satellite and receiver. Geodetic accuracy can be acquired from

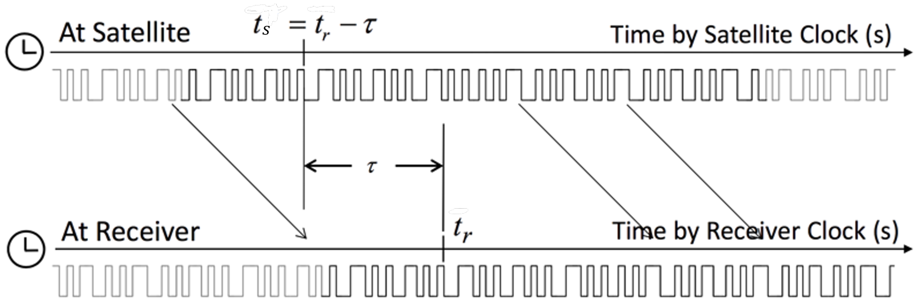

Figure 3.5: *Pseudorange Model (Takasu, 2013)*

code measurement by performing other corrections apart from measuring the geometric distance between satellite and receiver (ρ) and the clock synchronous error of receiver (dt_r) and satellite (dT_s). Other terms that need to be taken into accounts such as the error that occurs from the propagation of the signal through the atmosphere which is ionospheric (I) and tropospheric (T) delay, and the measurement errors (ϵp) include the multipath effect, receiver's and satellite's instrumental delays (European Space Acency, 2018). Therefore, the pseudorange that represents GNSS code measurement can be written as follows (Takasu, 2013) :

$$\begin{aligned} R_\mathrm{p} &= c((tr + dt_\mathrm{r}(t_\mathrm{r})) - (t^\mathrm{s} + dT_\mathrm{s}(ts))) + I + T + \epsilon p \\ &= c(t_\mathrm{r} - t_\mathrm{s}) + c(dt_\mathrm{r}(t_\mathrm{r}) - dT_\mathrm{s}(t_\mathrm{s})) + I + T + \epsilon p \\ &= \rho + c(dt_\mathrm{r}(t_\mathrm{r}) - dT_\mathrm{s}(t_\mathrm{s})) + I + T + \epsilon p \end{aligned} \tag{3.2}$$

The correction of these errors enables the code measurement to obtain an accuracy of around a few meters and can be improved to a meter by using augmentation systems such as WAAS (USA) or EGNOS (Europe). (European Space Acency, 2018; Vu, 2019).

Carrier Phase Measurement

Carrier phase measurement is the measurement of the range between a satellite and receiver based on the phase shift. The phase of the signal transmitted by the satellite is compared between a replica that the receiver generates (O'Driscoll, 2010). Phase shift measures the cycle fraction which is the offset between signals from the satellite and the replica generates by the receiver at time t. The signal that reaches the antenna receiver is a complete integer number of complete cycles N and the portion of the waveform that is only the part measured by the receiver which is known as the phase of the signal ($\Delta\varphi$). The information of the integer number of cycle N is unknown to the receiver, hence it is called integer ambiguity. As the receiver measures the signals continuously the phase shift φ can be calculated (Perez-Ruiz & K., 2012; Vu, 2019). The phase shifts φ at time t between carrier signal and replica can be computed as:

$$\varphi(t) = \Delta\varphi(t) + n(t) + N \tag{3.3}$$

$n(t)$ is the number of cycles proceeding from the start of measurement. The phase shift (φ) measurement can be seen from the fig.3.6. As the phase measurement can be calculated, the distance

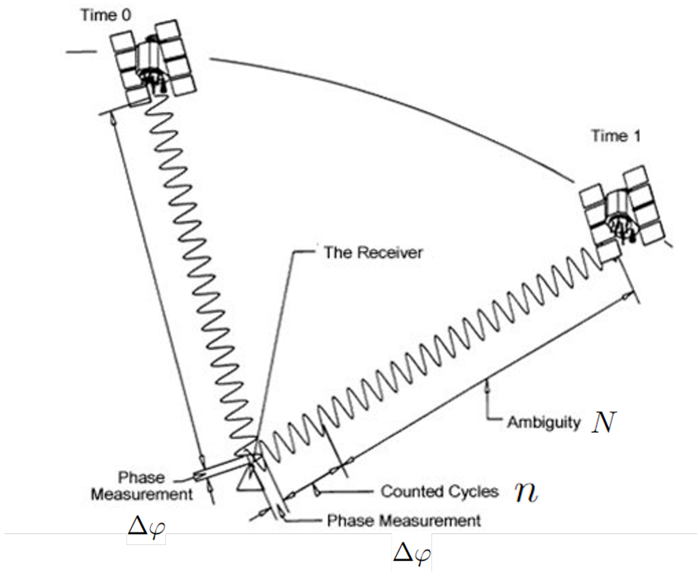

Figure 3.6: *Principle of Carrier Phase Measurement (Perez-Ruiz & K., 2012)*

between the satellite and the receiver can be computed. The carrier phase measurement can provide rage accuracy up to millimetres which is much smaller as the wavelength of the L1 carrier wave is 19 cm which can act as an accurate reference compared to code measurement (Perez-Ruiz & K., 2012).

3.3 GNSS SIGNAL STRENGTH INFORMATION

Signals from the satellite are transmitted in the radio frequency (RF) spectrum. The atmosphere and other natural objects such as trees, mountains as well as artificial e.g. buildings can impede signals from the satellite and cause delay (Oxley, 2017; Vu, 2019). As it is known that signals from GNSS satellite constellations are electromagnetic waves hence, when they encounter certain objects they will be reflected, scattered, absorbed and attenuated (National Aeronautics and Space Administration, Science Mission Directorate, 2010).

The signal strength received by a receiver antenna is measured in SNR (Wang, Zhang, & Zhang, 2018). The formula is SNR = PR/PN, with the signal power and noise power being the numerator and denominator, respectively. The GNSS receiver's SNR data for all frequencies (such as GPS L1/L2 or BDS B1/B2/B3) and all multipath effects can be independently examined for all visible satellites (Bilich & Larson, 2008). As a result, SNR data can be used to quantify multipath effects. The modulated signal of SNR(C/N) obtained from the receiver can also be referred to as Carrier to noise ratio (C/N). It is defined as a ratio between carrier signal power (C) to noise power (N) and is usually represented in decibel-hertz (dB Hz). To be consistent the term SNR will be used to refer to this.

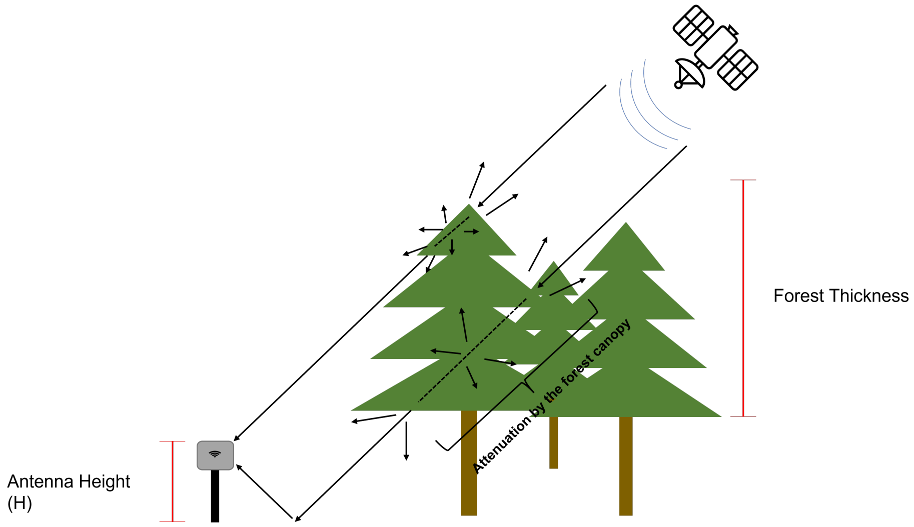

Figure 3.7: *The signal received by the antenna under the forest canopy*

3.3.1 GNSS signal Scattered and attenuated by the Forest Canopy

The strength of carrier signal power (C) of SNR is affected by the scattering away of signal that results in signal attenuation through the forest canopy while the strength of the noise (N) is affected by the scattering that results in multipath. The multipath effect in certain conditions can result in sinusoidal oscillation due to its dependency on the surface reflector. Under the forest canopy, the multipath effect will affect the GNSS signal where the signal will be scattered and attenuated due to the properties of the tree e.g., leaves, branches etc. The attenuation due to the multipath effect caused by the tree's properties can be recorded through SNR. The signal received by the antenna installed under the canopy can be illustrated as (figure 3.7). The signals penetrating through the forest will reach the forest floor however, due to the impact of the forest canopy which has scattered and attenuated the signals, the impact of reflected signals from the forest floor is assumed to be insignificant. This is similar to the approximation made for the upward model on L-band microwave emission that it mainly consists of vegetation and sky components hence, the emission from the forest floor by the soil could be neglected (Jennifer P. Grant et al., 2008).

It has been well documented through published studies that vegetation especially forests significantly affect the L-band satellite frequency. Thus, the forested area is usually left out for the retrieval of soil moisture from the forest floor. Some of the soil moisture retrievals were rather performed for the less dense forest type (Della Vecchia, Saleh, Ferrazzoli, Guerriero, & Wigneron, 2006). However, the results only indicated the potential of soil moisture retrieval which still required further experiments. In the case of the denser forests, the sensitivity towards the retrieval of soil moisture decreases (Della Vecchia, Ferrazzoli, Wigneron, & Grant, 2007; J. P. Grant et al., 2007). Kurum et al. (2012) Investigated the effect of vegetation at L-band, acknowledging that the scattering due to the attributes of forest canopy such as branches and trucks is significant and needs to be evaluated. Furthermore, the forest canopy attribute such as vegetation water content also impacts the L-band signals, particularly if the vegetation water content $> 5kgm^{-2}$. The high vegetation water content will not enable the L-band radiometer from reaching the accuracy of 0.04 $cm^3.cm^{-3}$ of soil moisture (Entekhabi, Njoku, & O'Neill, 2009).

The significant impact of the forest canopy on the L-band signals can be applied to the GNSS signals as well as it is transmitted in the same frequency. This impact has given an idea to focus on retrieving information from the forest canopy. Therefore, several studies have been published related to the attenuation of SNR such as the study on correlating GNSS signal response towards the effect of forest canopy (Guerriero et al., 2020; Liu et al., 2017), attenuation of L-band signals by vegetation (Wright et al., 2008). Furthermore, Rodriguez-Alvarez et al. (2012) has attempted to retrieve vegetation water content using GNSS measurement by analysing the attenuation power of the GNSS signals.

The principle applied by Liu et al. (2017) to get the information of the forest attribute was by analysing the GNSS signals penetrating through the forest. Two antenna receivers were installed where one was installed under the canopy and the other was under the open sky. The signal strength in terms of carrier-to-noise ratio (C/N) received by the two receivers was compared and showed that the receiver that was placed under the forest canopy had lower signal strength. The study analysed the GNSS features related to the attenuation of the signals through the forest and correlate them with the forest variables. The prediction of forest attributes from GNSS signal measurements was given an accuracy similar to the spectrometry and aerial photographs. In fact, in terms of RMS and correlation coefficient, GNSS signal measurements gave higher prediction compared to satellite-based 2-D techniques.

Attenuation due to atmosphere

One of the sources of error in GNSS positioning is attributed to the atmosphere. The GNSS signals travel a long way through the atmosphere before the signals reach the antenna receiver. The signals that travel through the atmosphere will experience some changes which cause the error in the accuracy of GNSS. Two regions that can alter and change the GNSS signals are the ionosphere and troposphere.

The ionosphere is one of the regions of the atmosphere where the free electrons can be found as they occur from the ionisation of the radiation from the sun. The radio frequency (RF) i.e., GNSS signals travelling through the ionosphere will be disturbed by the free electrons which will induce an error. The error can vary from a few meters at the low elevation angle (horizon) to around tens of metres at the high elevation angle (zenith) (Macgougan, Lachapelle, Nayak, & Wang, 2001).

The ionosphere is a dispersive medium that can contribute to delay depending on the frequency of the signals. The ionosphere dispersive property impacts the codes and carrier waves differently hence, it will cause the group delay where the code P and C/A are slowed or delayed while the carrier phase will be speeded up. However, the dispersive property causes refraction that is dependent on the frequency enable to correct the delay through dual frequency (L1 & L2). The degradation/attenuation of GNSS signals can be caused by the ionosphere which is known as scintillation due to plasma irregularity and density fluctuation. This effect mostly occurs in the equatorial, auroral and polar cap zone and it has seasonal dependence (J. Sanz Subirana, J.M. Juan Zornoza and M. Hernández-Pajares, Technical University of Catalonia, Spain., 2011; Macgougan et al., 2001).

The troposphere is the lowest layer of the atmosphere extending from the earth's surface to the altitude of 60 km. The troposphere is the opposite of the ionosphere which is non-dispersive for RF. The effects caused by the troposphere on GNSS signals are signal delay, attenuation and a small portion of scintillation (Macgougan et al., 2001). As it is non-dispersive the effects due to refraction become non-frequency dependent which is unable the correction for the error using dual frequency as the ionosphere. The refraction on the GNSS signals causes the delay which can be mitigated using a model or estimating it from the observational data. The delay through the troposphere can be modelled based on the wet and dry components of the troposphere. The dry component is caused by dry gasses such as nitrogen and oxygen while the wet component is caused by water vapour and clouds hence, it depends on the weather (J. Sanz Subirana, J.M. Juan Zornoza and M. Hernández-Pajares, Technical University of Catalonia, Spain., 2011).

The attenuation of the GNSS signals through the troposphere depends on the elevation angle of the observer (antenna receiver). The water vapour, rainfall and gasses such as nitrogen and oxygen in the troposphere also cause the attenuation however, it is insignificant (Macgougan et al., 2001).

Attenuation due to Forest Rainfall Interception

Based on the past studies above there is a potential to explore the attenuation of the GNSS signals due to rainfall interception by the canopy. Rodriguez-Alvarez et al. (2012) in their study could provide an approximation to infer a factor related to forest opacity and vegetation water content which showed the good agreement between the ground-truth and GNSS measurements of the leave with the correlation (r) of 93%.

In the case of rainfall interception, the forest canopy will intercept the portion of precipitation which is expected to add more to the effect of scattering and attenuation caused by the presence of water on the tree leaves and branches. The presence of water on the tree leaves and branches is believed to impact the GNSS signals in the form of signal loss due to attenuation.Gernot (2007) Observed the GPS signals using water as the medium and showed that 1 mm of water is sufficient to block GPS signals or greatly decrease the signal amplitude. Although it was a completely different setting, this can be related to the presence of water in the canopy which is interesting to be observed and understand.

3.3.2 Multipath Effect

The signal from the satellite which is reflected and scattered will change direction and create a multipath. As this signal travels a longer path, it will take a longer time to arrive at the antenna receiver (Vu, 2019). These signals will have different amplitudes relative to the direct signals and will result in certain delays and phases. The GNSS accuracy for positioning degrades by multipath, hence for positioning the multipath effects are a source of error and have to be mitigated (Jin et al., 2014).

The multipath effects on the GNSS signal depend on the environment around the GNSS antenna receiver. Hence, It has been discovered that a specific type of GNSS multipath can be used to sense the surface condition of the earth (Jin & Komjathy, 2010). Reflected signals which regard as the source of error for positioning purposes contain crucial information that can be obtained through the GNSS reflectometry technique. The properties around the antenna receiver can be traced back by isolating the reflected signals (Vu, 2019). This concept was first suggested for altimetric measurements by Martin-Neira (1993). Since then, this method has become a new alternative as a remote sensing tool. It has been tested and utilized for different applications. GNSS-R has been

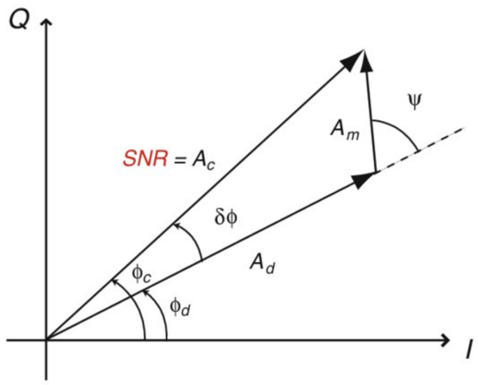

Figure 3.8: The phasor diagram illustrates the carrier tracking loop on the received GNSS signal under direct and multipath effect or reflected signals. The quadrature and in-phase components of the signal are specified in Q and I axes respectively. There are three phasor indicated as A_d, A_m, and A_c which are amplitudes of the direct, multipath and the composite of signals respectively.ϕ_d, ϕ_c, $\delta\phi$ respectively are phase of direct, composite signals and the phase error due to multipath. The relative phase of multipath is specified as ψ which is relative to direct amplitude (Larson et al., 2008)

used to retrieve various geophysical properties of the earth surface i.e., sea ice thickness (Komjathy et al., 2000), sea level (Lowe et al., 2002; Martin-Neira, 1993), soil moisture (Masters, 2004), etc.

3.3.3 Signals to Noise Ratio (SNR) for GNSS-Reflectometry

The signals received by the GNSS antenna are quantified through the amplitude of SNR. Most of the GNSS receivers derive SNR from the carrier tracking loop. The carrier tracking loop is lining up the locally generated carrier with the incoming signal (Hafidhi & Boutillon, 2016). The carrier tracking loop was described under the simplified model using a phasor diagram (Bilich & Larson, 2007; Ward, 1997) which illustrates the relationship between the I (in phase) and the Q (in quadrature). The diagram shows the component of received signals. In the case of no reflected signals or multipath effects, the diagram will only contain a direct signal which is the amplitude phasor of A_d. The carrier phase of A_d corresponds to ϕ_d . As it has been explained in phase carrier measurement, the phase of the signal transmitted by a satellite is compared to a replica from receiver (O'Driscoll, 2010) hence, any mismatch will result in a non-zero phase angle of ϕ_d . By keep tracking the ϕd, the carrier phase of GNSS signals can be calculated. In a theoretical case where there is no multipath effect, SNR will equal to the direct phasor (signal), SNR $= A_\mathrm{d}$.

When the multipath effect exists the additional phasor is added to the diagram which is the amplitude of multipath A_m. With the presence of the multipath effect, the carrier tracking loop will lock on the composite of signals amplitude A_c and its phase ϕ_c. This composite signal is the sum of the vector of all phasors which are direct and multipath, hence the measurements of the composite signal amplitude are equal to SNR (A_c = SNR). According to the model in the (figure 3.8, the bias or the phase error due to multipath $\delta\phi = \phi_\mathrm{c}$ - ϕ_d, then based on the law of cosine, SNR with the presence of direct and reflected signals or multipath can be described as follows (Bilich & Larson, 2008):

$$SNR^2 = {A_\mathrm{c}}^2 = {A_\mathrm{d}}^2 + {A_\mathrm{m}}^2 + 2A_\mathrm{d}A_\mathrm{m}cos\psi \tag{3.4}$$

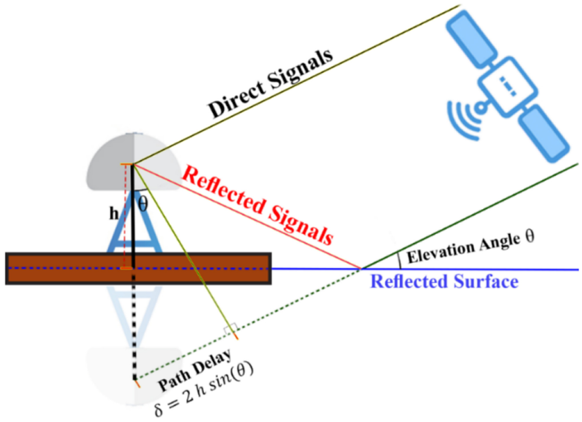

Figure 3.9: Geometry model of GNSS reflectometry in the case of a planar reflector. h is the height of the antenna concerning the planar reflector and θ is the elevation angle (Farzaneh, Parvazi, & Shali, 2021)

The geometrical model of SNR with the effect of multipath can also be simplified in the case of the reflection of a planar reflector. This model has enabled various studies to retrieve information related to ocean altimetry, soil moisture, sea ice thickness etc.

In the case of a planar reflector, the additional distance travelled by the reflected signal is $\delta = 2h$ sin (θ) as seen in the (Put figure) h and θ correspond respectively to antenna height relative to a planar reflector and downward looking angle which is technically the same as elevation angle. So, the phase shift caused by the multipath effect $\delta\phi$ can be written as follows (Elosegui et al., 1995):

$$\delta\phi = \frac{2}{\lambda}\delta = (2\pi\frac{2h}{\lambda}sin(\theta)) \tag{3.5}$$

By isolating the reflected signal or multipath the SNR of multipath is a function of amplitude A and cosine of the phase shift by the multipath $\delta\phi$ and the phase offset Φ. The formula can be expressed as follows (Larson, Löfgren, & Haas, 2013):

$$SNR_{\text{multipath}} = Acos(\delta\phi + \Phi) \tag{3.6}$$

Subsequently, the SNR of the reflected signals or multipath on the horizontal planar reflector can be expressed as follows:

$$SNR_{\text{multipath}} = Acos(\frac{4\pi h}{\lambda}sin(\theta) + \Phi) \tag{3.7}$$

3.4 CARRIER TO NOISE SIGNAL AS AN UNDERVALUED SOURCE OF GEOPHYSICAL INFORMATION

The noise of the signal transmitted by the GNSS satellite is recorded by the antenna receiver as a carrier-to-noise ratio. Attenuation affects the strength of the carrier signal while reflected signals (multipath) affect the noise strength. For positioning purposes, these effects are something to correct and avoid.

The attenuation which degrades signals is caused by several things such as the atmosphere and forest canopy. Due to this impact on the GNSS signals, some methods and models are used for the correction. However, attenuation for the GNSS signals can be used as the source of information to predict forest attributes such as biomass, tree mean height, and stem volume (Liu et al., 2017). Furthermore, Guerriero et al. (2020) investigated the GNSS signals attenuation by analysing the fluctuation of signals received by the antenna placed under the canopy to estimate forest biomass. Therefore, the attenuation of the GNSS signal has the potential to be used for the presence of water in the canopy e.g., rainfall interception.

For positioning purposes, the multipath effects cause noise that decreases the accuracy. The noise caused by the reflected signals (multipath) has to be mitigated for better accuracy of positioning. However, GNSS reflectometry reverses this paradigm by isolating the reflected signals to retrieve various geophysical information about the earth as mentioned in the section on multipath above.

Chapter 4

Study Area, Data & Methodology

4.1 STUDY AREA

Speulderbos is situated on a forest-rich elevated area (1100 Km**2**) named Veluwe in the province of Gelderland in the Netherlands (figure 4.1). The Speulderbos forest is located at 52°15'08" N, 5°41'25" E, at an elevation of 52 above NAP (m), within a large forested area in the Netherlands. In this study area, there is a scaffolding tower (47.4m) within a dense 2.5 ha Douglas fir (Pseudotsuga menziesii) stand, a type of evergreen needle leaf species (Raj, Alexander Samuel Hamm, Van Der Tol, & Stein, 2016). The area used to be sand dunes and at the end of the nineteenth century, reforestation began. The current stand of the forest canopy was planted in 1962 from 2 years old seedlings. According to the study conducted by Cisneros Vaca et al. (2018), the height of the forest canopy was around 34m, and the stem density and mean diameter at breast height (DBH) respectively were 571 tree/ha, and 34.8($\pm$8.9) cm, meanwhile the leaf area index (LAI) was 4.5 m^2/m^2. Based on this study, the amount of interception by the forest canopy was 38% of gross rainfall.

A GNSS antenna receiver is installed 11 m above the ground on the tower. The Speulderbos site is currently in use as a NitroEurope site which is the project for integrated Europen research into the nitrogen cycle and is also part of the global ForestGEO network of the large-scale forest-dynamics plot ("Speulderbos", n.d.). The Speulderbos site has several advantages such as the land features a sizeable homogeneous forest cover. Also, it is easily accessible for measurement and represents a large part of the forest in the Netherlands.

4.2 DATASETS & INSTRUMENTS

4.2.1 Dataset

There were two datasets used in developing this study namely, GNSS signals and meteorological data which are described as follows:

GNSS Signals

Commercial GNSS chips often use National Marine Electronics Association (NMEA) format to log the GNSS signals. NMEA data format contains SNR data which is usually not used but it

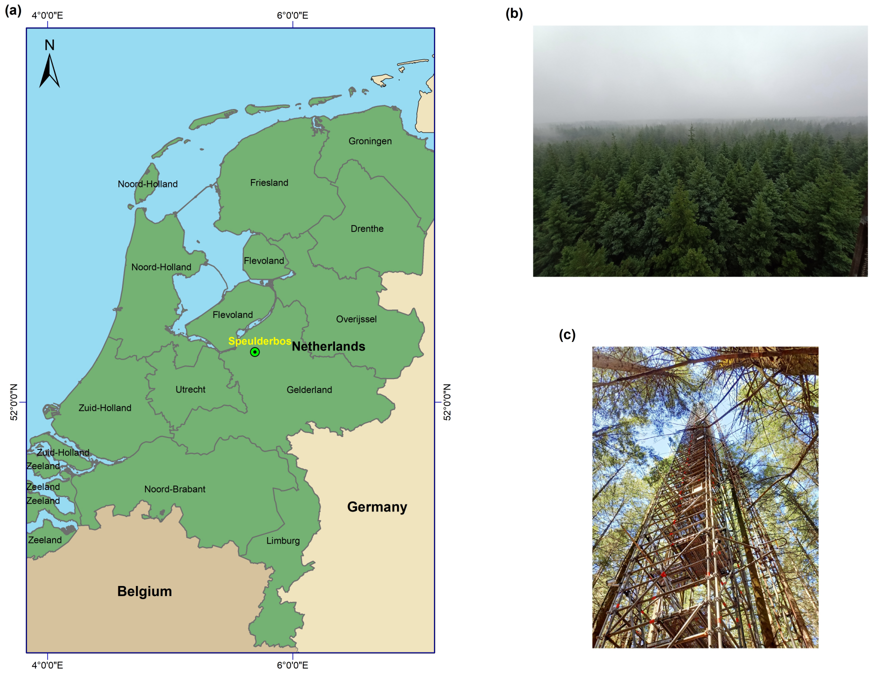

Figure 4.1: Study area in Speulderbos: (a) Location map in the Netherlands; (b) Speulderbos satellite view (c) a 47.4m scaffolding tower; (d) top view of the canopy.

contains valuable information. For each visible GNSS satellite, the GSV phrases of the NMEA format are directly used by the mass-market receiver to deliver integer numbers for elevation, azimuth, and signal-to-noise ratio (SNR). The GNSS NMEA is a standard data format for converting measurement data from a sensor to a predetermined American Standard Code for Information Interchange (ASCII) format that is supported by all vendors. It can output position, velocity, time, and satellite-related data in the case of GNSS (for the constellations that the antenna can de-code). There are several NMEA messages or sentences that provide integer values for elevation, azimuth, and signal-to-noise ratio, and GSV phrases constitute one of them (Martín, Ibáñez, Baixauli, Blanc, & Anquela, 2020). GSV phrase which includes messages from GPS can be seen in the (figure 4.2) and the description in the table

```
$GPGSV,4,1,15,195,59,162,39,05,53,288,45,42,51,129,36,02,49,348,41*4E
$GPGSV,4,2,15,19,49,149,42,06,42,065,43,13,29,187,37,12,24,254,33*75
$GPGSV,4,3,15,17,23,149,50,09,14,041,32,25,09,294,37,30,08,119,36*7E
$GPGSV,4,4,15,07,05,090,29,193,,,40,194,,,38*45
```

Figure 4.2: GSV phrase for GPS

Meteorological Data

To derive rainfall interception (I) some meteorological data were used. These meteorological data were obtained from the Royal Netherlands Meteorological Institute (KNMI). These meteorological data include hourly rainfall data, temperature, and global radiation (incoming shortwave radiation) within the period of this study experiment (March 26th to June 26th 2022). The meteorological

Table 4.1 The description of GSV phrase based on the figure 4.2 (https://cdn-shop.adafruit.com/product-files/5186/5186_PA1616D_Datasheet.pdf)

Name	Example	Units	Description
Message ID	$GPGSV		GSV protocol header
Number of Messages	4		Range 1 to4 (Depending on the number of satellites tracked, multiple messages of GSV data may be required.)
Message Number1	1		Range 1 to 4
Satellites in view	15		
Satellite ID	195		Channel 1 (Range 1 to 32) Note: 193∼195 for QZSS
Elevation	59	degrees	Channel 1 (Maximum 90)
Azimuth	162	degrees	Channel 1 (True, Range 0 to 359)
SNR (C/No)	39	dBHz	Range 0 to 99, (null when not tracking)
....	....	....	...
Satellite ID	07		Channel 4 (Range 1 to 32)
Elevation	05	degrees	Channel 4 (Maximum 90)
Azimuth	090	degrees	Channel 4 (True, Range 0 to 359)
SNR (C/No)	29	dBHz	Range 0 to 99, (null when not tracking)
Checksum	*4E		
<CR><LF>			End of message termination

data were obtained from 3 different stations. These stations are Lelystad (station 269) which is located at 52.458 °N, 5.526 °E and an elevation of -3.70 NAP (m), De Bilt (station 260) is located at 52.100 °N, 5.180 °E and an elevation of 1.90 above NAP (m), the other station is Deelen (station 275) which is located at 52.056 °N, 5.873 °E and an elevation of 48.20 above NAP (m). These data can be accessed through https://www.knmi.nl/nederland-nu/klimatologie/uurgegevens.

4.2.2 Instrument

We have acquired components (figure 4.3) that were used to build my receiver. The set of instrument combinations includes Raspberry pi, a GPS hat module and a low-cost mass-market GPS L1 antenna.

The GPS hat module used in this study is the CD-PA1616D GNSS patch antenna module. The CD-PA1616D GNSS patch antenna module was used to process the signals transmitted by the GNSS satellites. This antenna module uses NMEA format to log the GNSS signals and the description of NMEA output sentences within this product is shown in the table 4.2. The SNR (C/No) obtained through the NMEA sentence is in the dB-Hz unit. The specification of this module can be seen in the table 4.3.

The Raspberry pi used in this study is the Raspberry pi model B+. This model features (https://cdn-shop.adafruit.com/datasheets/pi-specs.pdf:

- Broadcom BCM2835 ARM!! 700MHz
- Mounting points and 512MB SD RAM

- 4x USB 2.0 connector
- MicroSD slot
- Dimensions of 85x56x17mm
- Micro USB socket 5V, 2A
- GPIO connector with 40-pin 2.54 mm

Table 4.2 The description of NMEA output sentences (https://cdn-shop.adafruit.com/product-files/5186/5186_PA1616D_Datasheet.pdf)

Option	Description
GGA	Time, position and fix type data.
GSA	GNSS receiver operating mode, active satellites used in the position solution and DOP values.
GSV	The number of GNSS satellites in view, satellite ID numbers, elevation, azimuth, and SNR values.
RMC	Time, date, position, course and speed data. Recommended Minimum Navigation Information.
VTG	Course and speed information relative to the ground.

The steps of setting up the instrument are explained as follows:

- Raspbian operating system (OS) was installed on raspberry pi by putting the microSD card into the card slot. This microSD should have been written with the raspbian disc image so the raspbian will boot directly when the raspberry pi is connected to the desktop.
- GPS hat module can be connected on top of the raspberry pi through the pins header on the board which connects the GPS hat to the serial ports of the raspberry. The GPS module has a GPS antenna connector to connect it to the low-cost mass-market GPS L1 antenna.
- Raspberry pi was programmed in python to command messages through the RX pin which is described as serial data input for firmware update (UART TTL) that is connected to the GPS module and to obtain NMEA output through the TX pin (serial data output for NMEA Output (UART TTL). The script can be accessed through https://gitlab.utwente.nl/s2466627/raspberry_gnssr.

4.3 METHODOLOGY

The methodology of this study aims to observe the detectability of forest canopy interception through SNR recorded by the GNSS antenna. The overall workflow to achieve this can be seen in the (figure 4.4).

4.3.1 Instrument preparation and installation

The workflow starts with the instrument preparation where the components were acquired to build the low-cost GNSS antenna, this process has been explained in the instrument section of the previous chapter. Before the antenna was installed, it was important to know where the source of

Table 4.3 The description of the CD-PA1616D GNSS patch antenna module (https://cdn-shop.adafruit.com/product-files/5186/5186_PA1616D_Datasheet.pdf)

Item	Description
GNSS Solution	MTK MT3333
Frequency	GPS L1, 1575.42 MHz GLONASS L1, 1598.0625 ∼ 1605.375MHz
SV Number	#1 ̃32 for GPS #65 96 for GLONASS #1 36 for Galileo #193 195 for QZSS #33 51 for SBAS
Update Rate	1 Hz (default), maximum 10 Hz
Baud Rate	9600 bps (default)
Position Accuracy	Without aid: 3.0m (50% CEP) DGPS(SBAS(WAAS,EGNOS,MSAS,GAGAN)): 2.5M (50& CEP)
Velocity Accuracy	Without aid: 0.1m/s DGPS(SBAS(WAAS,EGNOS,MSAS,GAGAN)): 0.05m/s
Timing Accuracy (1PPS Output)	±20 ns RMS within 100ms in one pulse
Altitude	Maximum 18,000m (60,000 feet)
Velocity	Maximum 515m/s (1000knots)
Acceleration	Maximum 4G
Power supply	VCC: 3.0V to 4.3V ; VBACKUP: 2.0V TO 4.3V
current consumption @ 3.3V, 1Hz Update Rate	Acquisition: 34mA, Tracking: 29mA
Working temperature	-40°C to +85°C
Dimension	16 x 16 x 6.7 mm, QNF
Weight	6g

reflected signals comes from based on the height of the antenna. This can be done through Fresnel's plot. GNSS-R reflection zone is shown in Fresnel's zone which shows the sensing zone in elliptical shapes(figure 4.5). The size of these elliptical zones depends on the height of the antenna (H_R), satellite elevation angle (e) and transmitter frequency (L1). When the satellite raises the elevation angle increase and the Fresnel zones get smaller and get closer to the antenna (Roesler & Larson, 2018). The equation for a Fresnel zone can be seen in the appendix of Larson and Nievinski (2013).

Due to the GPS satellite orbital plane, the sky in a certain location is not all covered by the GPS satellite (figure 3.9). It is important to see how many GPS satellites orbit over the sky of our observation area. In this study, the area of interest is filtered based on the azimuth from 0°to 120°. This area was chosen for the reason that this part of the forest is quite homogeneous and the GNSS antenna was installed in the north right corner of the tower (figure 4.6). The tower frame also could be an issue that can interfere with GNSS signals if the area of interest is expanded to more than 120°. As we know that the northern sky of the study area is not covered by the satellite so it

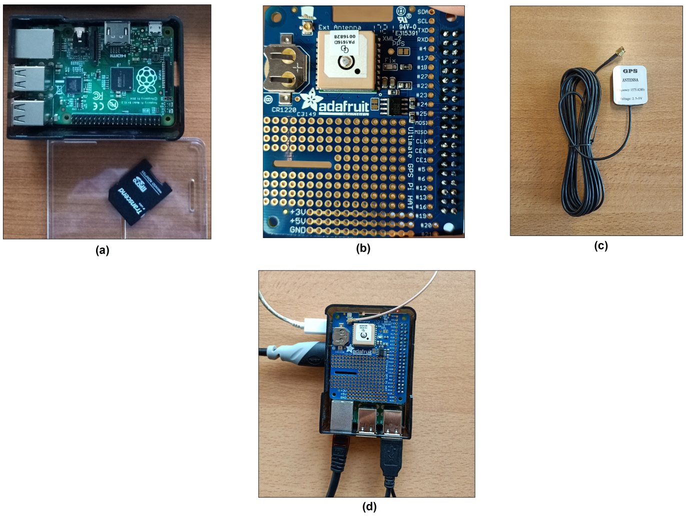

Figure 4.3: (a) Raspberry pi; (b) GPS hat module; (c) low-cost mass-market GPS L1 antenna; (d) Instrument combination (Captured by : Christian Sarungallo)

is not necessary to be added.

The low-cost GNSS antenna was installed below the canopy on the tower at a height of 11 m from the ground. The antenna was placed below the canopy (figure 4.8) to observe the scattering and attenuation effect from the tree and also how it changes as the canopy intercept some portion of the precipitation.

4.3.2 SNR data processing

GNSS antenna that was installed under the canopy in the Speulderbos was continuously recording direct signals from the satellite as well as the reflected signals. The GNSS chips used the NMEA format to lock the signals. The data that contain SNR was processed using python and the script can be accessed through https://gitlab.utwente.nl/s2466627/MSC_DATA_ANALYSIS. There were two scenarios developed related to azimuth angle and elevation angle for SNR data processing as follows:

Scenario I

The area of interest for the observation has been explained in the previous section hence data were filtered based on the azimuth angle of 0-120 °4.7. Only the SNR value from the satellites that pass through this azimuth will be selected.

The signals from low elevation angles and high elevation angles were removed from the data, hence the only signals used were coming from 20 to 70 degrees. This was performed due to the low elevation angle of SNRs contains more error while the high elevation angle is assumed to contain more direct signals from the satellite. As described in the figure 4.8, the SNR with a low elevation angle will travel the longer path of the forest, hence the signals will mostly be scattered and attenuated before arriving at the receiver.

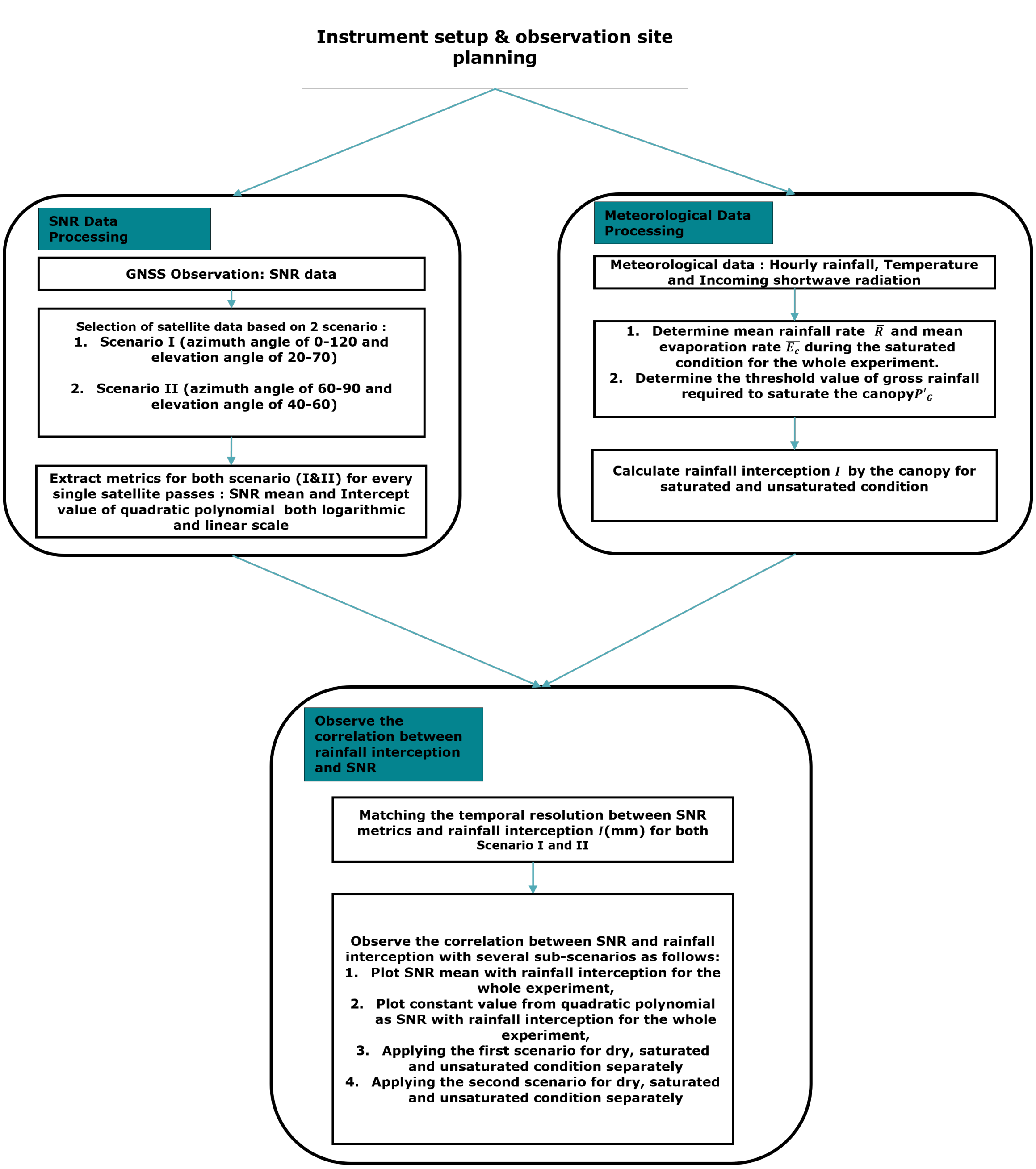

Figure 4.4: Methodology workflow

Scenario II

The concern of the assumption of the homogeneity of the forest motivated the development of the second scenario by reducing the area of interest 4.9 based on the azimuth of 60-90°. In the case of scenario I, some of the single passes of satellites were only visible at certain elevation angles for example 20-40°which will not be comparable to 40-60°as the SNR value depends on elevation angle. Therefore, the elevation angle range was reduced to 40-60°in this scenario.

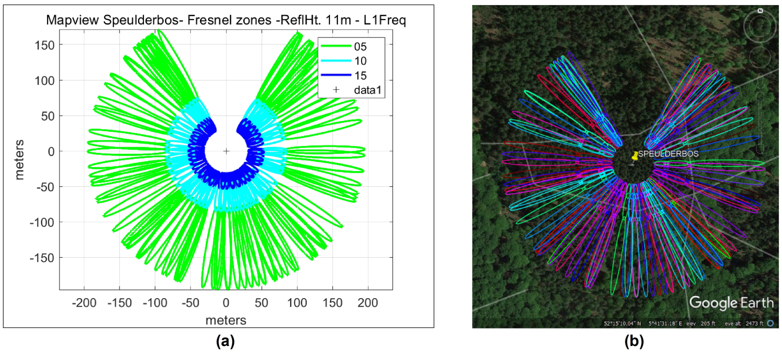

Figure 4.5: (a) Fresnel zones in mapview for GNSS site Speulderbos. Elevation angles are 5,10 and 15 which are indicated in green, cyan and blue respectively. An HR value of 11 m was used; (b) Screenshot of first Fresnel zones for GNSS site Speulderbos with the reflection zone for elevation angle of 5,10 and 15 projected on a Google Earth image. An HR of 11 was used as well (created using Matlab codes by Roesler and Larson (2018))

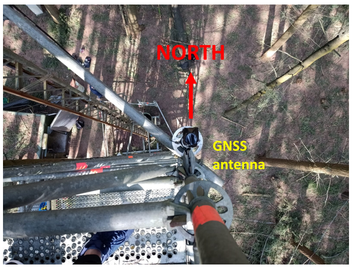

Figure 4.6: GNSS antenna Installed on the tower 11 m above the ground

4.3.3 Extracting Metrics for SNR

Logarithmic Scale (dB-Hz)

The next step was to process the SNR data for each visible satellite pass. The SNR(C/N) value is represented in dB Hz which is determined as follows:

$$SNR_{\text{dB}} = 10log_{10}(\frac{C}{N}) = C_{\text{dBm}} - N_{\text{dBm}} \tag{4.1}$$

where C is carrier signal power and N is noise power. The SNR value of each pass of a satellite was averaged to get the mean value. The effect of scattering which results in attenuation and multipath will affect the magnitude of the SNR. The bigger the effect of attenuation and multipath will result in low SNR and in the opposite case, the SNR will be higher and it can be also seen through the mean of the SNR. The mean of SNR value for one satellite pass was calculated as follows:

$$SNR_{\text{mean}} = \frac{Sum\ of SNR}{Number\ of\ SNR} \tag{4.2}$$

$$SNR_{\text{elev\_i}} = \frac{Sum\ of i\_low\ to\ i\_high}{Number\ of\ SNR} \tag{4.3}$$

SNR_{mean} equals the sum of SNR from the low elevation to the high elevation divided by the number of SNR with respect to the elevation angle.

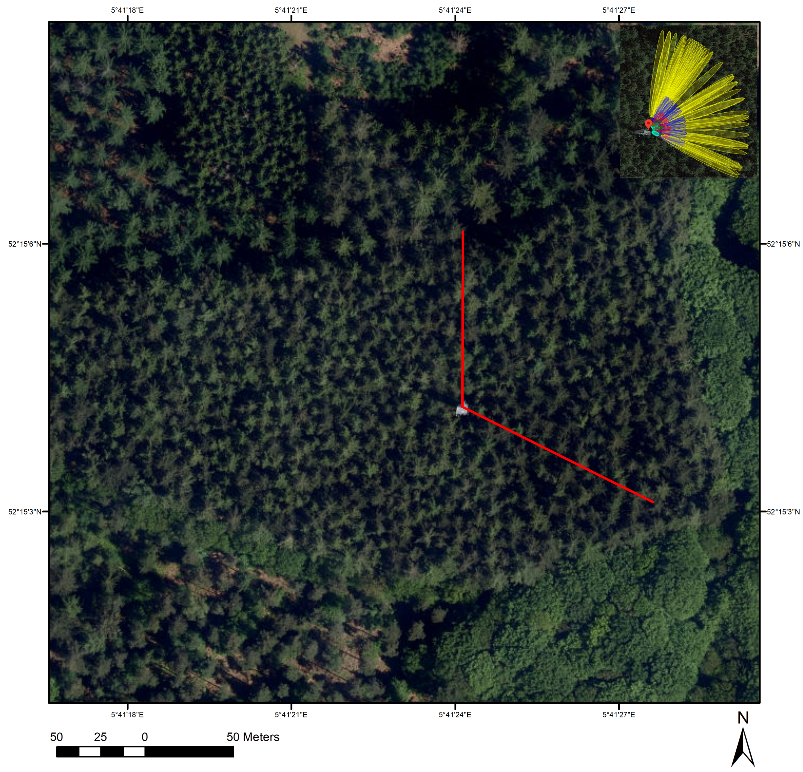

Figure 4.7: *Area of interest based on the azimuth of Scenario I*

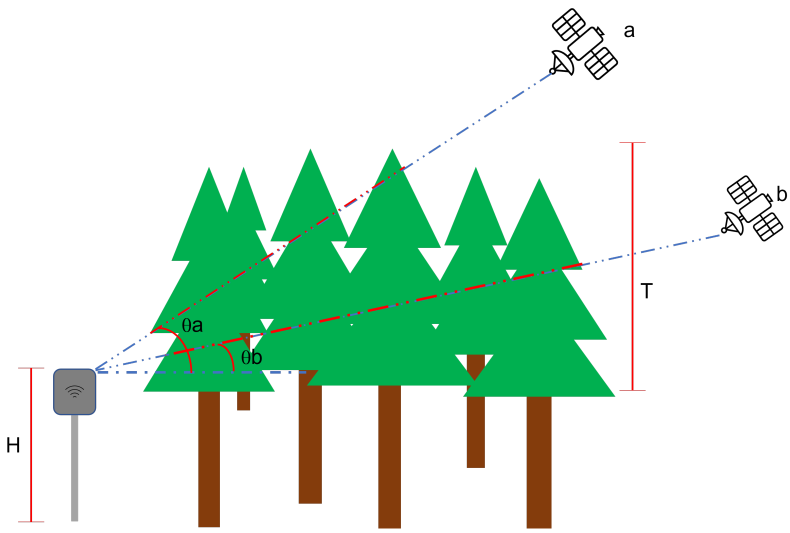

Figure 4.8: *GNSS Signals Received by the antenna under the forest canopy. The signal from the satellite (a) with the high elevation angle (θa) travels a shorter part of the forest canopy compared to satellite (b) with the low elevation angle (θb) hence, mostly the signals from low elevation angle will be scattered and attenuated. H is antenna height from the ground and T is canopy thickness.*

As illustrated in the figure 4.8, SNR depends on elevation angle and antenna height. The signal received from a low elevation angle travels through the longer path through the forest which results in more attenuation and multipath effect as the signal will be mostly scattered. This will result

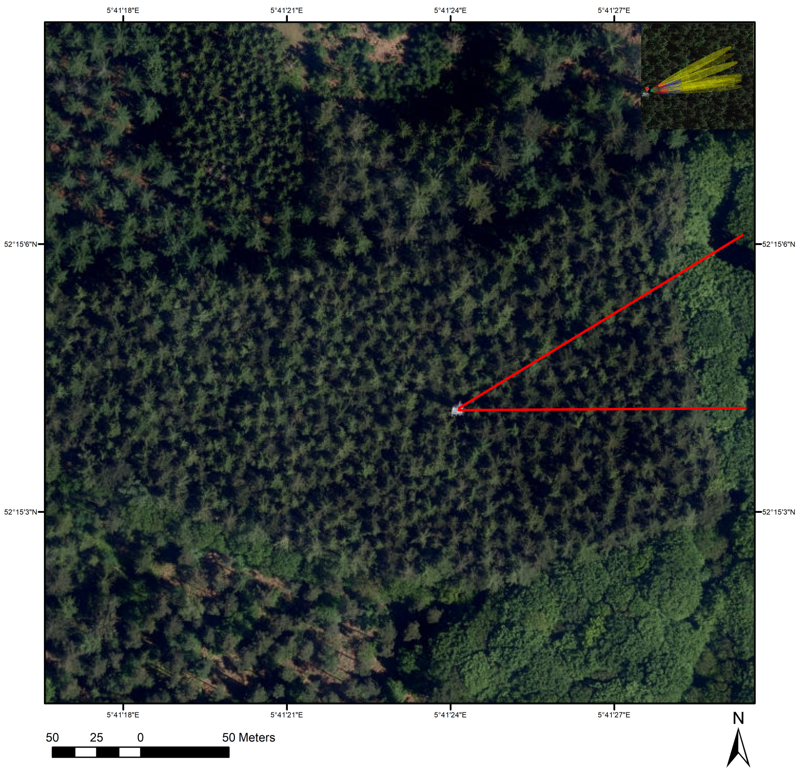

Figure 4.9: *Area of interest based on the azimuth of Scenario II*

in a low SNR value compared to a signal from a higher satellite angle. The signal will travel a short distance through the forest canopy from a higher elevation angle, hence the SNR value is higher. Therefore, the SNR values with respect to elevation angle will show an increasing trend (figure4.11b). In this case, representing SNR mean could be less ideal hence, the other alternative was to extract metrics from the constant value of the quadratic polynomial plot. The standard form of the quadratic polynomial equation is written as:

$$y = ax^2 + bx + c \tag{4.4}$$

$$SNR_\theta = a\theta^2 + b\theta + c \tag{4.5}$$

the y and x variables correspond to SNR and elevation angle respectively. c value equals to y intercept. In this case, x value which is the elevation angle (θ) has been filtered from 20 to 70 °for scenario I and 40-60°for scenario II hence, the median value was used for each pass of the satellite. Thus, c value is y (SNR) value that corresponds to x when x equals to median (elevation angle). Therefore, the constant value from quadratic polynomial can be used as a metric to represent SNR due to the influence of elevation angle towards the distance path through the forest canopy.

The SNR metrics obtained from the SNR data processing correspond to the whole area of interest of the forest, in the other words, it is assumed that the area of interest is homogeneous.

Linear Scale (Volt/Volt)

Similar to the logarithmic scale (dB-Hz), by following the same steps the metrics were extracted to represent SNR for each satellite pass for linear scale (volt/volt) as well. This was done by converting the logarithmic scale to linear (figure 4.10) first as follows:

$$SNR_{\text{dB}} = 10log_{10}(\frac{V_{\text{C}}}{V_{\text{N}}})^2 = 20log_{10}(\frac{V_{\text{C}}}{V_{\text{N}}}) \tag{4.6}$$

Hence,

$$SNR_{\text{volt/volt}} = 10^{\text{SNR}_{\text{dB}}/20} \tag{4.7}$$

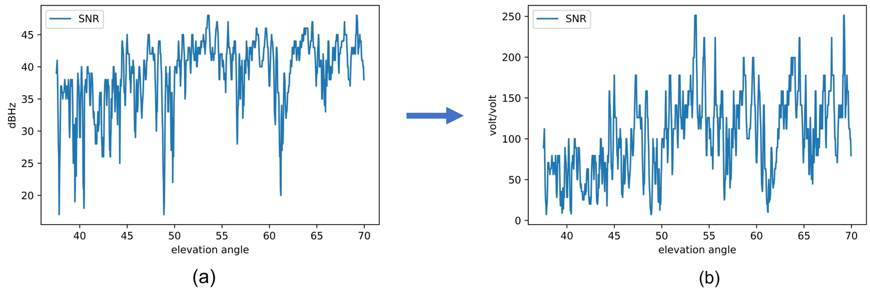

Figure 4.10: (a) SNR data with respect to elevation angle in (dB Hz) and (b) in linear scale (volt/volt)

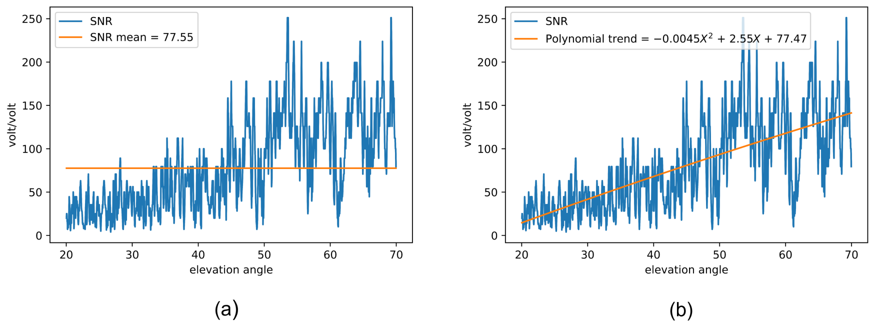

Figure 4.11: (a) SNR metric which shows mean of SNR for a single pass of satellite and (b) quadratic polynomial plotting to extract constant value as the metric of SNR for a single pass of a satellite

4.3.4 Rainfall interception by forest canopy

In this methodology, rainfall interception was estimated using one of the physical-based models, an analytical model of rainfallGash et al. (1995). The forest rainfall interception was calculated by determining the threshold value of the rainfall that can saturate the canopy P'_{G} using the equation(2.1) and then interception could be calculated based on the saturation of the canopy using equation (2.2) and (2.3). There were some assumptions or conditions applied to calculate rainfall interception by forest canopy and they are elaborated as follows:

1. S_c which is canopy storage is directly derived from the measurement of canopy storage in Speulderbos using IEA (individual event analysis) (Cisneros Vaca et al., 2018) which is 1.90 mm. It is assumed that the canopy storage at the current condition would not change drastically since this measurement.

2. FVC which is fractional vegetation cover is the ratio of vegetation type in a particular area. The value of FVC used in this study is derived from the previous study (Hahirwabasenga, 2019) in the Veluwe area for coniferous forest (Douglas-fir) as the Speulderbos is the part of this forest area. The FVC tells the state of the land area whether it is densely or sparsely vegetated. The value of FVS is a ratio, hence it ranges from 0-1. The FVC value was obtained using the remote sensing technique from the sentinel-2 dataset from June to October 2016. The FVC value used in this study was the mean value of this period. The assumption is that the state of the forest will not change drastically compared to the current situation hence, this value was used.

3. $\bar{R}$ is the mean rainfall rate during the saturated condition that will be derived from KNMI meteorological data at Lelystad, De Bilt, and Deelen stations. $\bar{R}$ value will be measured only for the saturated condition ($P_G >$ 0.5mm/h) (Gash, 1979) and it will be measured for the whole period of experiment according to Gash et al. (1995) model.

4. $\bar{E}_c$ is the mean evaporation rate which was calculated for the saturated condition for the whole period of the experiment as well. The mean evaporation rate was calculated based on the Makkink reference evaporation. This method only requires the average air temperature and incoming shortwave radiation and at KNMI this is the method used to calculate evaporation (Hiemstra & Sluiter, 2011). The mean evaporation rate was calculated as follows:

$$ET_{\text{ref}} = C.\frac{s}{s+\gamma}.\frac{S^{\downarrow}_{\text{day}}}{\lambda * \rho} \tag{4.8}$$

ET_{ref} is the Makkink evaporation in (m/day), C is a constant which equals to 0.65, ρ is the bulk density of water which equals to 1000kg/m^3, The incoming radiation which is in (J/m^2/day) is described as $S^{\downarrow}_{\text{day}}$

s is the slope of the curve saturation water vapour pressure in (kPa°/C). It is related to the mean daily temperature and can be described as follows:

$$s = \frac{7.5 * 237.3}{(237.3 + Tday)^2}.ln10.e_s \tag{4.9}$$

The saturation vapour pressure e_s(hpa) equals to:

$$e_s = 0.6107 * 10^{\frac{7.5Tday}{237.3+Tday}} \tag{4.10}$$

γ is a psychometric constant:

$$\gamma = 0.0646 + 0.00006T_{\text{day}} \tag{4.11}$$

λ is the heat of vaporisation:

$$\lambda = (2501 - 2.375T_{\text{day}}) * 1000 \tag{4.12}$$

In this study, the mean evaporation rate during the saturated condition was calculated based on KNMI meteorological data with hourly resolution. The only data required to measure evaporation based on Makkink are T_{hour} and $S^{\downarrow}_{\text{hour}}$

4.3.5 Observe the correlation between rainfall interception and SNR

Before the correlation between rainfall interception and SNR was performed, the Temporal resolution of SNR has to be matched with meteorological data for rainfall interception. The SNR has a temporal resolution in minutes to a few hours during a single pass of a satellite while the meteorological data has an hourly resolution, hence the mean value of meteorological data during the period of a single pass of the satellite was used.

The next step was to perform some other sub-scenarios from scenarios I and II to observe the correlation between Interception loss and SNR. These scenarios are described as follows:

1. Plot an SNR metric which is the (SNR_{mean}) against interception loss (I) and examines the correlation,
2. Plot an SNR metric which is the constant value from quadratic polynomial against interception loss (I) and examine the correlation,
3. Applying the first scenario above only for a saturated condition where $P_{\text{G}} > P'_{\text{G}}$ and unsaturated condition where $P_{\text{G}} < P'_{\text{G}}$, and dry condition when there is no interception
4. Applying the second scenario above only for a saturated condition where $P_{\text{G}} > P'_{\text{G}}$ and unsaturated condition where $P_{\text{G}} < P'_{\text{G}}$, and dry condition when there is no interception.

Chapter 5

Results

5.1 INTERCEPTION LOSS ESTIMATION

5.1.1 Meteorological and forest Parameter

The interception loss in the case of Douglas-fir (coniferous forest) in the Speulderbos was estimated based on several meteorological and forest state parameters. Rainfall and evaporation parameters were derived based on data from three different stations (De Bilt, Lelystad and Deelen). The forest state parameters used in this study were derived from the previous studies and can be seen in the table 5.1.

Table 5.1 The forest state parameter values of canopy storage derived from Cisneros Vaca, Van Der Tol, and Ghimire (2018) and fraction vegetation cover of the coniferous forest at the Veluwe area by Hahirwabasenga (2019)

Forest State	**Value**
Canopy Storage	1.9 mm
Fraction Vegetation Cover (FVC)	0.45

The estimation of interception loss was based on Gash et al. (1995) model and the evaporation was calculated using the Makkink reference 4.8(Hiemstra & Sluiter, 2011). The overall interception loss during the period of 26th March to 26th June was 35% of overall gross rainfall (213.73mm). The interception loss was estimated based on the rainfall events (P_G>0.5mm). The summary of the estimation of parameters and interception loss can be seen in the table 5.2.

To get some insight into how the distribution of the rainfall and interception loss throughout the period of the study, it can be seen in the table 5.3 and figure 5.1. June was the highest gross rainfall of 76.1 mm while March is the lowest. The rainfall events in March were not recorded for the whole month hence, it was the lowest one but the highest interception loss of the rainfall took place during this period. The amount of interception loss is influenced by canopy storage Fraction Vegetation Cover (FVC) as the interception loss depends on the capacity of the vegetation to retain the water due to the rainfall.

Table 5.2 The summary of meteorological parameters and interception loss estimation in this study

Parameters	**Estimated Values**
Overall rainfall of the entire period of the study (mm)	213.73
Overall mean of evaporation (mm/h)	0.21
$\bar{R}$ mean rainfall (mm/h) during saturated period P_G>0.5mm	1.66
$\bar{E}_c$ mean evaporation (mm/h) during saturated period	0.039
P'_G threshold value needed by the rainfall to saturate the canopy (mm/h)	4.27
I Interception loss (mm)	75.2
I Interception loss (%) of the overall rainfall of the entire period of the study	35%

Table 5.3 Monthly rainfall and interception loss in the period of 26 March to 26 June

Period	**Rainfall (mm)**	**Interception loss (mm)**	**Interception loss(%)**
March (26th - 31th)	18.43	7.11	38.56
April	56.90	18.90	33.22
May	62.3	21.40	34.35
June (1th - 26th)	76.1	27.79	36.52

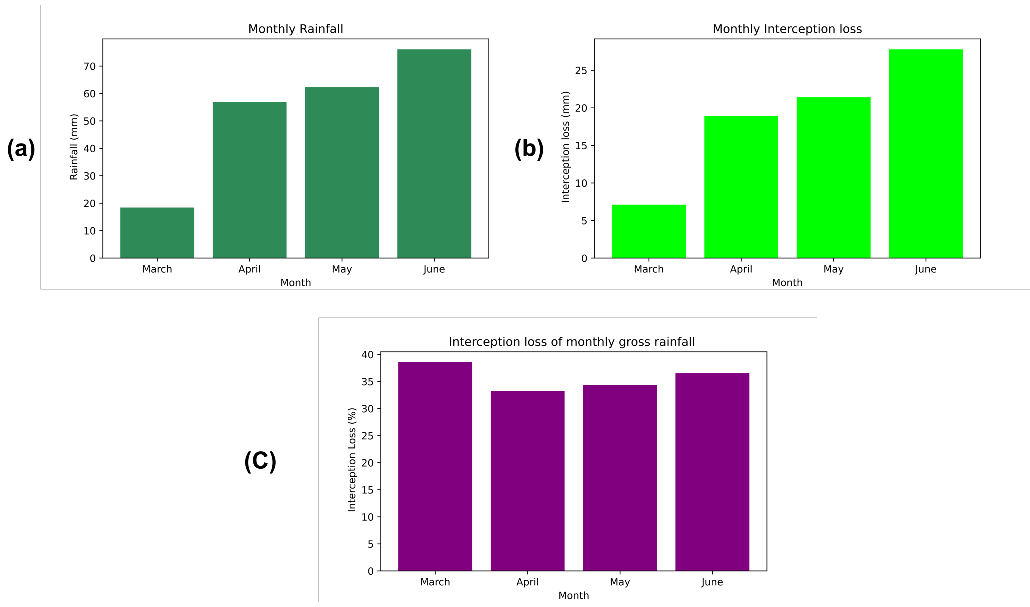

Figure 5.1: Monthly rainfall and interception from the average value of 3 different stations (Lelystad, De Bilt, and Deelen) during the study

5.1.2 Comparison between measured and estimated Interception loss

In order to verify the estimated interception loss, the measured interception loss from the previous study by (Cisneros Vaca et al., 2018) was used. This study was conducted in two different growing seasons i.e., June to October 2015 and 2016. This study took place in the same location as the current study which was the Speulderbos. The interception loss and mean evaporation of this study are presented in the table 5.4.

Table 5.4 Measured Interception loss and mean evaporation (Cisneros Vaca, Van Der Tol, & Ghimire, 2018)

Interception loss June to October 2015	37%
Interception loss June to October 2016	39%
Mean evaporation rate	0.2 mm/h

The estimated value of interception loss and mean evaporation rate derived from this study are 35% and 0.21mm/h respectively. Based on the table 5.4, the results from this study are comparable. However, It has to be noted that the similarity and differences of the results from both of the studies can be associated with the period of the study as well as the model and parameters used in both studies which will be further explained in Chapter 6.

5.2 MATCHING THE TEMPORAL RESOLUTION OF METEOROLOGICAL DATA AND SIGNAL TO NOISE RATIO (SNR) METRICS DATA

The temporal resolution of both meteorological data and Signal to Noise Ratio (SNR) from GNSS measurement was different. In order to find the relationship between both Interception and SNR data, they have to be matched.

The meteorological data is recorded hourly while the SNR data is based on the single pass of the satellite which can take from a few minutes to a few hours. The meteorological data were matched into SNR data by taking the value within the period of SNR data of the single pass of a satellite. If the single pass of a satellite takes a few hours then the mean value of the meteorological data will be used. There were two scenarios conducted to find the relationship between these two data. These two scenarios are elaborated as follows:

Scenario I

The scenario I developed in this study is based on the SNR measurements at the azimuth of 0-120°and elevation angle of 20 to 70°. This was decided as the north to the east part of the forest was considered more homogeneous. However, the drawback of choosing the northern part area is less visibility of the satellite due to their orbital plane. This has been explained in the chapter3 under the section3.1 and can be seen in the figure3.2.

The result of the meteorological parameters and interception loss after temporal resolution matching is shown in the table 5.5

Table 5.5 (Scenario I) Meteorological parameters and interception loss estimation after the temporal resolution has been matched with SNR data

Parameters	Estimated Values
Overall rainfall of the entire period of the study (mm)	307.92
$\bar{R}$ mean rainfall (mm/h) during saturated period P_G>0.5mm	1.60
$\bar{E}_c$ mean evaporation (mm/h) during saturated period	0.037
P'_G threshold value needed by the rainfall to saturate the canopy (mm/h)	4.27
I Interception loss (mm)	111.36
I Interception loss (%) of the overall rainfall of the entire period of the study	36.16%

After Matching the meteorological data with SNR data some parameters such as mean rainfall during the saturated period ($\bar{R}$), mean evaporation ($\bar{E}_c$), and threshold value needed by the rainfall to saturate the canopy (P'_G) and the percentage of interception loss (I(%)) remain almost the same with the original meteorological data 5.2. The increasing value of overall rainfall from 213.73mm to 307.92mm and interception loss from 75.2mm to 111.36mm are due to some of the satellite passing within the same period of time.

Scenario II

Scenario II was developed due to the concern of the assumption related to the homogeneity of the area chosen in the scenario I. In scenario II the data from the azimuth of 60-90°and elevation angle of 40-60°were used. By reducing the azimuth angle then the area of measurement will be smaller however, the SNR data obtained will be less.

The result of the meteorological parameters and interception loss after matching their temporal resolutions in this scenario II is shown in the table 5.6

Table 5.6 (Scenario I) Meteorological parameters and interception loss estimation after the temporal resolution has matched with SNR data

Parameters	Estimated Values
Overall rainfall of the entire period of the study (mm)	154.79
$\bar{R}$ mean rainfall (mm/h) during saturated period P_G>0.5mm	1.60
$\bar{E}_c$ mean evaporation (mm/h) during saturated period	0.034
P'_G threshold value needed by the rainfall to saturate the canopy (mm/h)	4.27
I Interception loss (mm)	57.86
I Interception loss (%) of the overall rainfall of the entire period of the study	37.38%

According to the table 5.6, the results are similar to the scenario I where the parameters of meteorological data remain the same as the original one 5.2. The value of overall rainfall and interception loss in mm decrease to 154.79 as the SNR data also decreases as a result of reducing the azimuth and elevation angle. At a certain time, there is no satellite data with the criteria of azimuth and elevation angle of this scenario II. As the result, some of the rainfall data is not included.

5.3 RELATIONSHIP BETWEEN INTERCEPTION LOSS AND SNR METRICS FROM GNSS MEASUREMENT

Relations between interception loss and SNR from GNSS measurement at the Speulderbos were examined after matching both of the temporal resolutions of the data. Interception loss data is represented in mm/h and the SNR data is represented in mean value and quadratic polynomial intercept value for both dB-Hz and Volt/Volt unit. The relationship between Interception and SNR from GNSS measurement is examined through two scenarios based on the azimuth and elevation angle as follows:

5.3.1 Scenario I (azimuth 0-120°and elevation angle 20-70°)

The metrics used for the SNR are the mean and the intercept value of quadratic polynomials from every single pass (descending or ascending) of the satellite as has been explained in the chapter 4 under the section 4.3.3. The metrics to represent SNR were both extracted from the logarithmic scale and linear scale.

Logarithmic Scale (dB-Hz)

The hypothesis related to SNR and rainfall interception was the negative correlation between the two (figure5.2a). The SNR value was expected to be higher during the dry period and lower during the saturated period. It was assumed that the presence of water in the canopy will attenuate the SNR value. However, this assumption can not be seen according to the figure 5.2 (b) and (c) for both SNR metrics (mean and intercept value of quadratic polynomial).

Based on the hypothesis, the SNR value was supposed to be higher during the dry period due to the less attenuated signals as there was no water present in the canopy. However, during the dry period, the SNR values are not accumulated in the high value but distributed across low to high values based on the figure 5.2 (b) and (c). This result can be attributed to the assumption that the forest of the study was homogeneous which is not necessarily true. The SNR data recorded by the low-cost GNSS antenna might pass through the thicker part of the forest hence, the SNR value was lower even in the dry condition.

The SNR metrics were further analysed by taking their median values for both of the metrics as presented in the table 5.7. Both SNR metrics which are the mean and intercept of the quadratic polynomial show a descent trend with respect to forest conditions from dry to saturated 5.3. However, it can barely be visible for the SNR metric from the intercept of the quadratic polynomial.

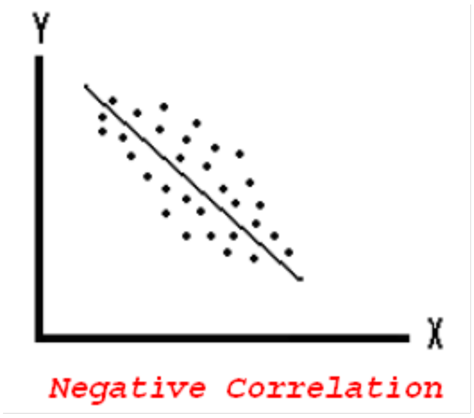

(a)
Hypothesis

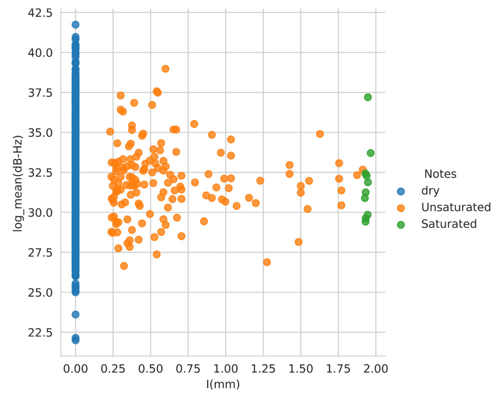

(b) Mean as SNR Metric

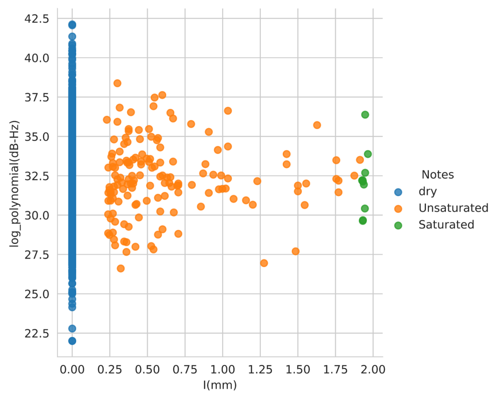

(c) Intercept of Quadratic Polynomial as SNR Metric

Figure 5.2: *(a). The hypothesis of the relationship between SNR value to interception loss (b). SNR, where mean, is used as a metric (dB-Hz) with respect to interception loss (mm) (c). SNR, where intercept from quadratic polynomial, is used as a metric (dB-Hz) with respect to interception loss (mm)*

Table 5.7 (Scenario I (dB-Hz)) median and mean value of SNR metrics based on the forest condition

	Dry		Unsaturated		Saturated	
	Mean	polynomial	Mean	polynomial	Mean	polynomial
Median	32.10	32.22	31.95	32.21	31.55	32.17

Linear Scale (Volt/Volt)

SNR data in logarithmic scale (dB-HZ) was converted to linear scale (Volt/Volt). Similar to the logarithmic scale, the mean and intercept of a quadratic polynomial of every single pass of the satellite were used as the metrics. The result as seen in the figure 5.4 also does not show any clear correlation.

The median value from SNR metrics of linear scale can be seen in the table 5.8 which is also visualised in figure 5.5. The SNR metric using the mean value shows a decreasing trend based

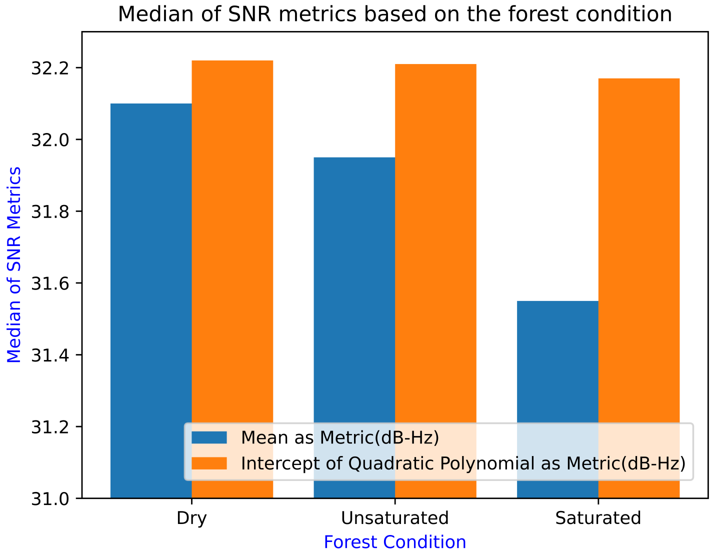

Figure 5.3: (Scenario I) Forest condition with respect to the median from SNR Metrics (dB-Hz)

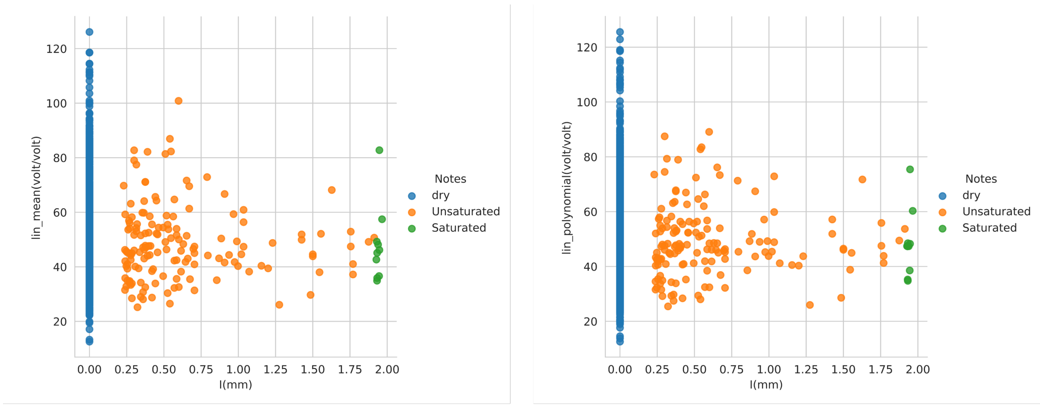

(a) Mean as SNR Metric

(b) Intercept of Quadratic Polynomial as SNR Metric

Figure 5.4: (a). SNR, where mean, is used as a metric (Volt/Volt) with respect to Interception loss (mm) (b). SNR, where intercept from quadratic polynomial, is used as a metric (Volt/volt) with respect to interception loss (mm)

on forest conditions from dry to saturated. In contrast, the SNR metrics using intercept of the quadratic polynomial show an increased value from the unsaturated conditions from 47.3 to 47.42.

Table 5.8 (Scenario I (Volt/Volt)) median and mean value of SNR metrics based on the forest condition

	Dry		Unsaturated		Saturated	
	Mean	polynomial	Mean	polynomial	Mean	polynomial
Median	47.87	47.45	46.58	47.3	45.65	47.42

The results from the scenario I do not show any significant correlation between SNR data from both logarithmic as well as linear scales using both mean and intercept of a quadratic polynomial

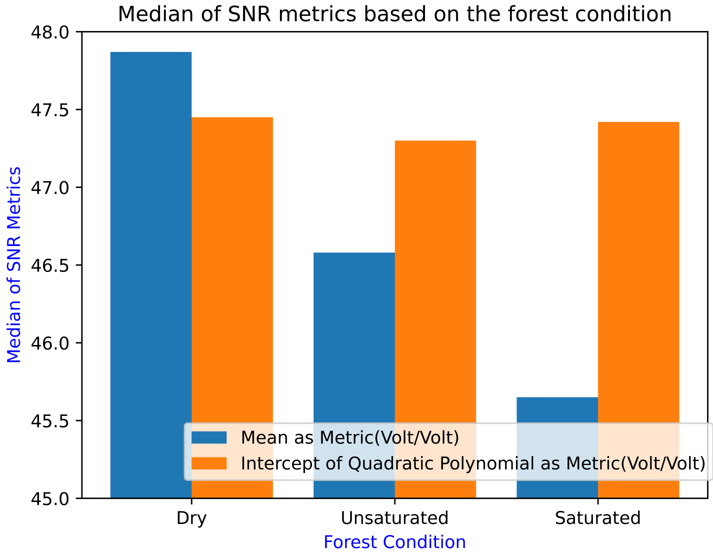

Figure 5.5: *(Scenario I)Forest condition with respect to the median from SNR metrics (Volt/Volt)*

as the metrics. The results of scenario I were assumed to be influenced by the assumption that the forest was homogeneous. Besides, there was a concern related to the elevation angle used in this scenario. The range of the elevation angle was considered large (20 -70°) where for some cases the single passes of satellites were only visible at certain elevation angles for example 20-40°which will not be comparable to a satellite passes at 40-60°as the SNR value depends on elevation angle. Therefore, these issues motivated to perform another scenario.

5.3.2 Scenario II (azimuth 60-90°and elevation angle 40-60°)

Scenario II was performed concerning the homogeneity of the forest and issue-related elevation angle in scenario I. To reduce the impact of the forest that may not be homogeneous as the assumption, the azimuth angle range was decreased to 60-90°. By reducing the azimuth range the area of the observed forest becomes smaller which resulted in less SNR data as well. However, both the result from the logarithmic (figure 5.6) scale and linear scale (figure 5.7) shows similar results as the scenario I. From the figure 5.6 and 5.7, The SNR value with respect to interception loss which was grouped into dry to saturated conditions did not show a specific pattern as the indication of a correlation.

Other factors that may influence this result are further elaborated in the chapter 6. Concerning the satellite's passes which only take a few minutes that would add more noise to the data, appendix A.1 and A.2 show both scenarios I and II that only take > 30 minutes length of passes of a single satellite into account. However, both scenarios still do not show any significant change except some of the low SNRs during dry periods are removed.

Logarithmic Scale (dB-Hz)

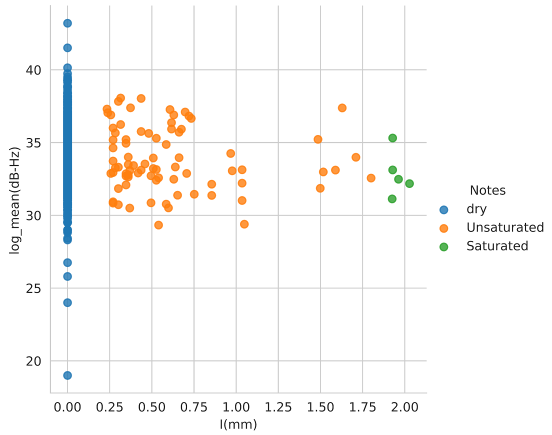

(a) Mean as SNR Metric

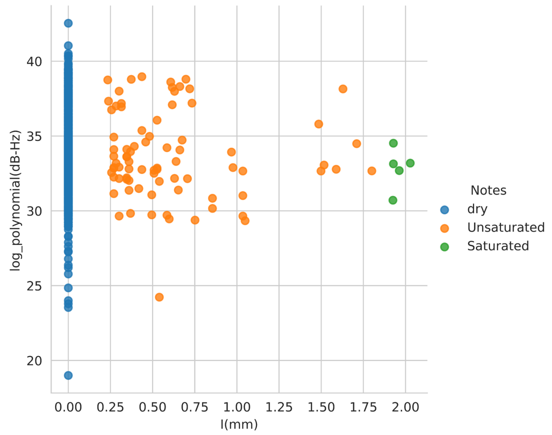

(b) Intercept of Quadratic Polynomial as SNR Metric

Figure 5.6: (a). SNR, where mean, is used as a metric (dB-Hz) with respect to interception loss (mm) (b). SNR, where intercept from quadratic polynomial, is used as a metric (dB-Hz) with respect to interception loss (mm)

Linear Scale (Volt/Volt)

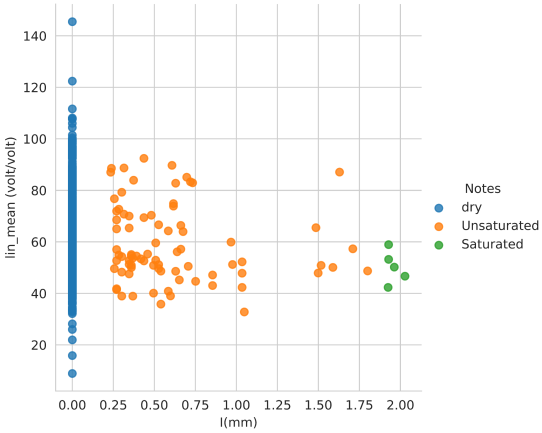

(a) Mean as SNR Metric

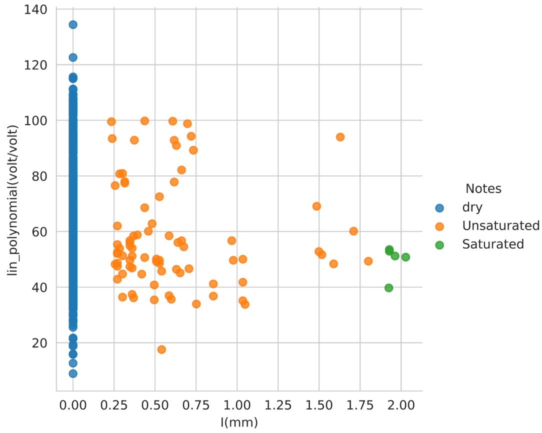

(b) Intercept of Quadratic Polynomial as SNR Metric

Figure 5.7: (a). SNR, where mean, is used as a metric (Volt/Volt) with respect to interception loss (mm) (b). SNR, where intercept from quadratic polynomial, is used as a metric (Volt/volt) with respect to interception loss (mm)

Chapter 6

Conclusions & Discussion

This study was carried out to observe the detectability of forest rainfall interception through SNR measurement using a low-cost GNSS antenna. The conclusion from this study is drawn based on the findings from the analysis. In this section, the conclusion is presented by providing elaboration and discussion related to the objectives of this study by answering the research questions as follows:

How to compute a representative interception estimate for the site based on the forest canopy information and meteorological data available?

The rainfall interception was estimated based on the model of Gash et al. (1995). The estimated interception loss in this study during the period of 26th March to 26th June 2022 was 35% of overall gross rainfall and the overall mean of evaporation was 0.21mm/h. The result of this study is slightly different but still comparable to the previous study by Cisneros Vaca et al. (2018) at the same location where the interception loss was 37% from June to October 2015 and 39% from June to October 2016 and the mean evaporation rate was 0.2mm/h.

In terms of comparability, it has to be noted that one of the forest parameters i.e., Canopy storage on the previous study Cisneros Vaca et al. (2018), was used in this current study which may induce the bias to the similar result for both of the study. Furthermore, this parameter may change as the measurement in the previous study was conducted a few years back where the state of the forest may be different compared to the current study.

In terms of the result is slightly different from Cisneros Vaca et al. (2018), apart from the different period of study, more parameters were used for their model to estimate interception loss. These parameters include the coefficient of throughfall which is the fraction of the rainfall that reaches the ground without touching the forest canopy and the coefficient which represents the fraction of rain diverted to the trunk and stems storage capacity.

The other forest state parameter which is Fraction Vegetation Cover (FVC) was derived from the study by Hahirwabasenga (2019) in the Veluwe area. This study obtained the FVC through remote sensing technique using sentinel-2 images during the period June to October 2016. The FVC from this study represent the coniferous forest (Douglas-fir) in the Veluwe area. The Speulderbos is also a coniferous forest however it only represents the small subset of the Veluwe area hence, using the FVC from this study may not be entirely accurate.

Furthermore, meteorological data used in this study were obtained from the mean value of three different stations close to the observed forest. The Interception loss measurement is preferable by using the in-situ data as the ideal representation data of the observed forest.

Despite the limitations of the data used in this study to estimate Interception loss, this study still shows a comparable result to the previous study and can be further evaluated based on the summary of other studies for Douglas-fir forest in table 6.1.

Table 6.1 The summary of interception loss for Douglas-fir forest, [a] Mixed Douglas-fir and Western hemlock. This table is adapted from Cisneros Vaca, Van Der Tol, and Ghimire (2018)

Reference	Interception loss (%)	Evaporation (mm/h)	Reference
Netherlands	38	0.077	Klaassen, Bosveld, and de Water (1998)
UK	39	NA	Rutter, Morton, and Robins (1975)
Belgium	30	NA	Soubie, Heinesch, Granier, Aubinet, and Vincke (2016)
US (north-western Pacific)[a]	21	0.25	Pypker, Bond, Link, Marks, and Unsworth (2005)
US (north-western Pacific)[a]	24	0.21	Pypker, Bond, Link, Marks, and Unsworth (2005)

In this study Interception loss was represented in mm with hourly resolution. However, the SNR data for a single pass (ascending or descending) of a satellite measured by the GNSS antenna has a temporal resolution that varied from a few minutes to hours. Integrating these two data by matching the temporal resolution may cause inaccuracy due to the inconsistency of the temporal resolution of a single pass of the satellite. As the result, the interception loss of 35% slightly changed to 36.16% and 37.38% for scenario I and scenario II respectively.

How useful are the metrics extracted from the SNR data?

SNR data from a single pass of the satellite was represented in the metrics by taking its mean, and intercept value extracted from quadratic polynomial plotted on the SNR with respect to elevation angle. The change of SNR value due to attenuation was assumed to be captured through the change of these two metrics. The motivation for choosing these two metrics has been explained in the 4 under the section 4.3.3.

The issue in the case of representing SNR of a single pass of a satellite in a metric was related to elevation angle. Not all satellite is visible to the antenna at the same elevation angle due to their orbital plane. In this study, two scenarios were developed related to filtering the elevation angle of measurements. The elevation angle of measurements was filtered from 20-70°for Scenario I. However, the SNR data obtained includes all ranges inside this preferred elevation angle. In certain cases, a single pass satellite has an elevation angle ranging from 20-40°and 40-60°. Therefore the SNR metrics, in this case, are not comparable and can be the source of the inaccuracy in this analysis. On the other hand, filtering the elevation angle exclusively to obtain the exact uniform data will result in less data which is not enough for the analysis. The concern related to elevation angle motivated to establish Scenario II with the range of elevation angle of measurement reduced to 40-60°. However, the data obtained will be less compared to scenario I. According to the result, the metrics extracted to represent SNR data in all scenarios established in this study have not given significant results that can show any correlation to interception loss (mm).

What is the correlation between forest rainfall interception and SNR data from low-cost antenna measurement?

Two scenarios were established in an attempt to find a correlation between SNR and interception from GNSS low-cost antenna measurements. Scenario I does not show any clear correlation between interception loss and SNR data based on the mean and intercept value of quadratic polynomial of the SNR for both logarithmic (dB-Hz) and linear (Volt/Volt) scales. It was expected during the dry condition when there is no interception loss the SNR would be accumulated at high values due to the less attenuation of the signal. However, the values are also distributed at the low SNR. The main concern related to this issue was the assumption that the observed forest was homogeneous. During the dry condition, some satellites might pass through the thicker part of the forest which resulted in a low SNR value due to the high attenuation of the forest canopy. Hence assuming that the forest was homogeneous can oversimplify the analysis that causes the inaccuracy.

The SNR values which were plotted against interception values were further analysed by taking the median according to the interception loss during the dry to the saturated condition of the forest. According to Scenario I using the logarithmic scale (dB-Hz) value both the mean and intercept of the quadratic polynomial show a trend that a high median value corresponds to the dry condition and low to saturated condition. The mean metric gives a median value of 32.10, 31.95, and 31.55 respectively for dry, unsaturated and saturated conditions. It is also similar to the intercept of quadratic polynomial metric, where it gives the median values of 32.22, 32.21, and 32.17 respectively for dry to saturated conditions. Furthermore, the linear scale (Volt/Volt) also gives the same trend using the mean as a metric but the intercept of the quadratic polynomial shows the median value of 47.42 during a saturated period which is slightly higher than an unsaturated one which is 47.3. However, the dry condition still gives the highest median value among other conditions. The median value of SNR metrics shows a slight trend related to forest conditions (dry, unsaturated, and saturate) which may be caused by the rainfall interception, however, the difference between the value is so negligible to conclude so and it could also be because of water in the troposphere.

Scenario II was established due to the concerns related to the assumption that the forest is homogeneous as well as the problem related to the elevation angle mentioned in the previous section. To minimise these issues the area of the observed forest was reduced by filtering the azimuth angle and elevation angle. However, the data obtained from this scenario became less than the previous scenario and it still gives a similar result related to SNR and interception loss.

What are the indications or findings to conclude whether the low-cost antenna can work for this study?

The hypothesis was made related to this study that there will be a negative correlation where SNR value will be high when there is no or less interception as the presence of the water in the canopy due to forest interception will attenuate the GNSS signals. However, both scenarios established in this analysis do not reflect this hypothesis. It has been elaborated in the previous section of this chapter where the issues may occur that influence the result of this analysis.

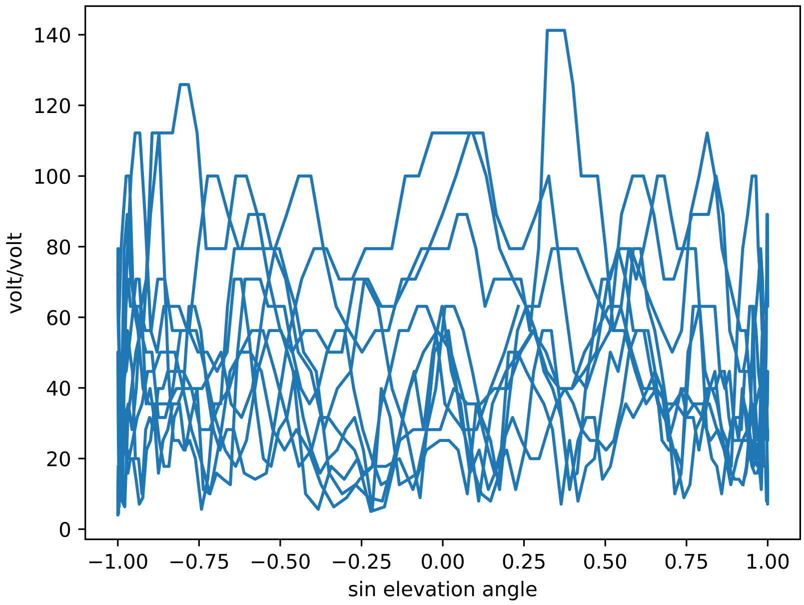

Figure 6.1: *SNR data from a single pass of the satellite with respect to sin elevation angle*

One of the others concerned is related to the planar reflector that might dominate the signals received by the antenna. However, it has been mentioned in the chapter 3 under the section 3.3.1 that the effect of the forest floor is negligible and could be neglected (Jennifer P. Grant et al., 2008). In fact, the signals obtained from this study do not show any significant oscillation that follows the sinusoidal trend as shown in figure 6.1. The signals are very noisy as they travel through the forest which scattered and attenuated the signals. As the signals are very noisy, it is hard or impossible to apply GNSS reflectometry to identify planar reflectors (Chew, n.d.).

The effect due to attenuation of the atmosphere 3.3.1 is assumed to be small, however, during the study, the antenna installed at the top of the canopy did not work. Therefore, the impact of the attenuation of the atmosphere cannot be measured which can also influence the result of this study.

In conclusion, this study does not give a significant indication related to the detectability of forest rainfall interception using the low-cost antenna. However, It has been elaborated related on the limitation, and challenges that influence the current study. Hence, it cannot be concluded yet whether the low-cost antenna works or does not work for the detectability of forest rainfall interception. The applicability of low-cost antenna can still be further investigated by solving and minimising the issues, challenges and limitations found in this study. The next chapter will elaborate on the recommendation based on these findings.

Chapter 7

Recommendation

The previous chapter has discussed the findings as well as the challenges and limitations that influence the current study. Based on those, some of the recommendations are given for the future direction related to this study as follows:

- The current study lacks in-situ measurement from the study area related to meteorological data. Hence, this could be solved by using meteorological data measured directly in the study area.
- Forest parameters such as storage canopy, Fraction Vegetation Cover (FVC) were derived from the previous study which does not reflect the current state of the study area. It is ideal to use the latest data related to these parameters.
- The impact of atmospheric attenuation remains unknown in this current study. Installing another antenna receiver above the canopy would allow atmospheric effects during the observation to be cancelled out when considering the difference in SNR of the top and bottom receivers.
- Outlier detection can be performed related to duration data of SNR (length of a single satellite's pass) to see how the short duration data affects the result. The short-duration data can be thrown out to clean the data.
- Another scenario that can be tried for the next study is using every single SNR data as an isolated proxy for interception loss instead of computing a metric per pass of the satellite.

Appendix A

Other figures

A.1 SNR DATA >30 MINUTES OF A SINGLE PASS OF A SATELLITE ON SCENARIO I

A.1.1 Logarithmic Scale (dB-Hz)

Logarithmic Scale (dB-Hz)

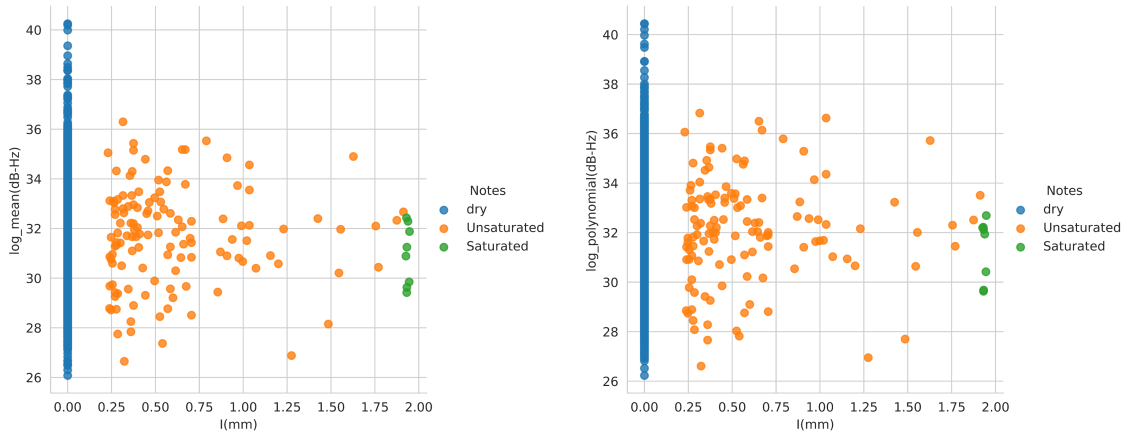

(a) Mean as SNR Metric

(b) Intercept of Quadratic Polynomial as SNR Metric

Figure A.1: (a). SNR, where mean, is used as a metric (dB-Hz) with respect to interception loss (mm) (b). SNR, where intercept from quadratic polynomial, is used as a metric (dB-Hz) with respect to interception loss (mm)

A.1.2 Linear Scale (Volt/Volt)

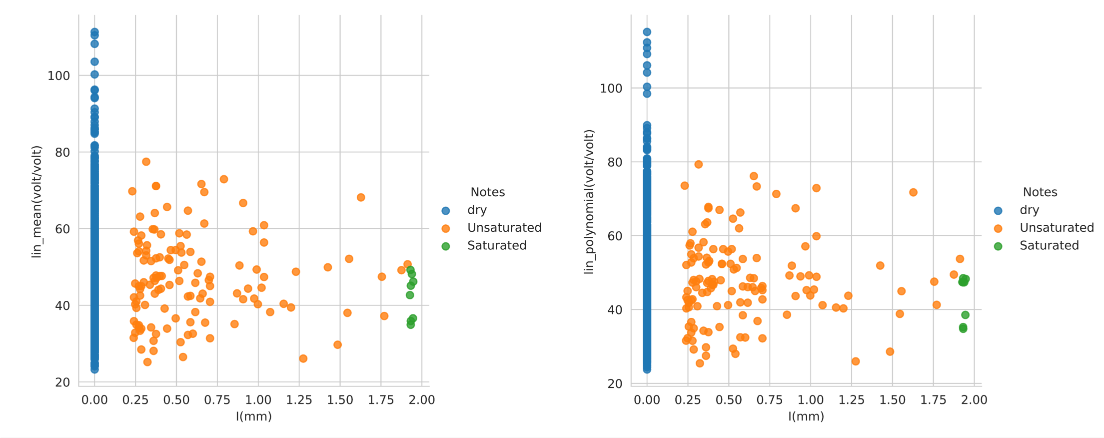

(a) Mean as SNR Metric (b) Intercept of Quadratic Polynomial as SNR Metric

Figure A.2: *(a). SNR, where mean, is used as a metric (dB-Hz) with respect to interception loss (mm) (b). SNR, where intercept from quadratic polynomial, is used as a metric (dB-Hz) with respect to interception loss (mm)*

A.2 SNR DATA >30 MINUTES OF A SINGLE PASS OF A SATELLITE ON SCENARIO II

A.2.1 Logarithmic Scale (dB-Hz)

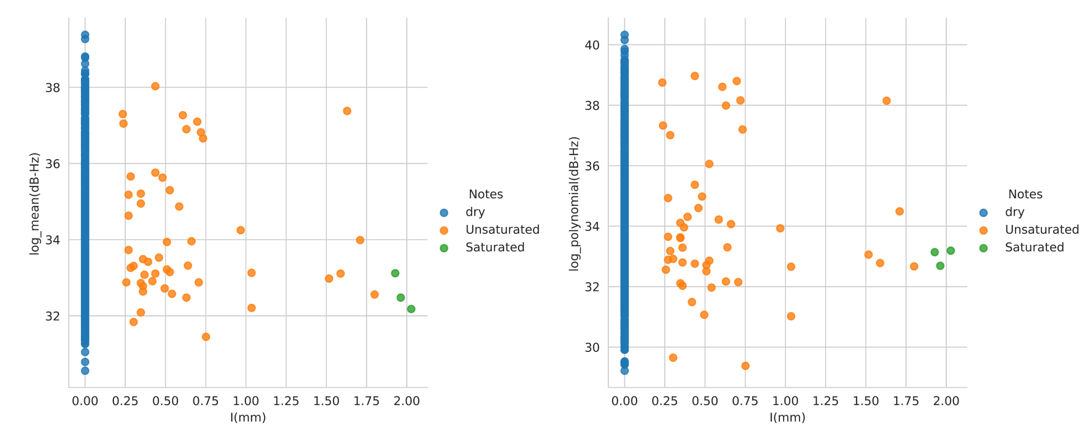

(a) Mean as SNR Metric (b) Intercept of Quadratic Polynomial as SNR Metric

Figure A.3: *(a). SNR, where mean, is used as a metric (dB-Hz) with respect to interception loss (mm) (b). SNR, where intercept from quadratic polynomial, is used as a metric (dB-Hz) with respect to interception loss (mm)*

A.2.2 Linear Scale (Volt/Volt)

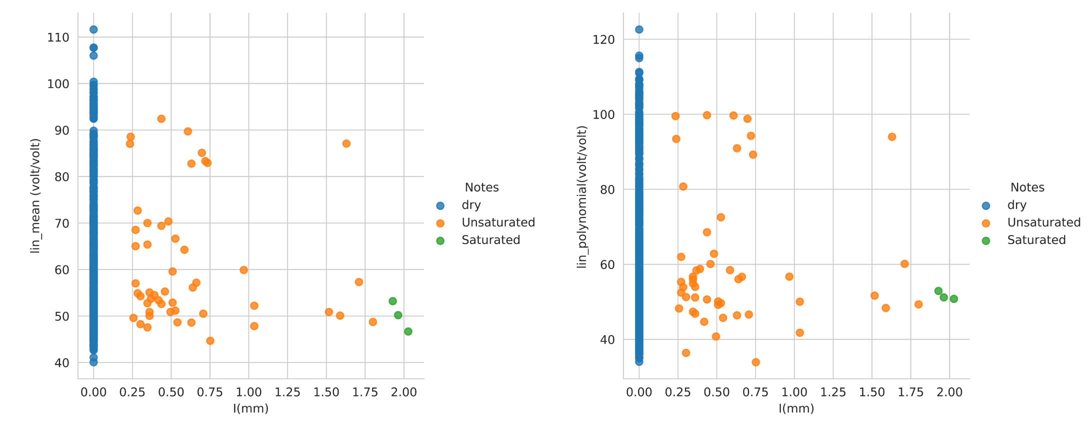

(a) Mean as SNR Metric

(b) Intercept of Quadratic Polynomial as SNR Metric

Figure A.4: *(a). SNR, where mean, is used as a metric (dB-Hz) with respect to interception loss (mm) (b). SNR, where intercept from quadratic polynomial, is used as a metric (dB-Hz) with respect to Interception loss (mm)*

List of References

Aston, A. (1979). Rainfall interception by eight small trees. *Journal of hydrology*, *42*(3-4), 383–396.

Balasubramaniam, R., & Ruf, C. (2020). Characterization of rain impact on l-band gnss-r ocean surface measurements. *Remote Sensing of Environment*, *239*, 111607. doi:10.1016/j.rse.2019.111607

Banskota, A., Kayastha, N., Falkowski, M. J., Wulder, M. A., Froese, R. E., & White, J. C. (2014). Forest Monitoring Using Landsat Time Series Data: A Review. *Canadian Journal of Remote Sensing*, *40*(5), 362–384. doi:10.1080/07038992.2014.987376

Beutler, G., Weber, R., Hugentobler, U., Rothacher, M., & Verdun, A. (1998). Gps satellite orbits. In P. J. G. Teunissen & A. Kleusberg (Eds.), *Gps for geodesy* (pp. 43–109). doi:10.1007/978-3-642-72011-6_2

Bilich, A., & Larson, K. M. [Kristine M.]. (2007). Correction published 29 march 2008: Mapping the gps multipath environment using the signal-to-noise ratio (snr). *Radio Science*, *42*(06), 1–16. doi:10.1029/2007RS003652

Bilich, A., & Larson, K. M. [Kristine M.]. (2008). Correction to “Mapping the GPS multipath environment using the signal-to-noise ratio (SNR)”. *Radio Science*, *43*(2). doi:10.1029/2008RS003839

Bonan, G. B. (2008). Forests and climate change: Forcings, feedbacks, and the climate benefits of forests. *science*, *320*(5882), 1444–1449.

Bryant, M. L., Bhat, S., & Jacobs, J. M. (2005). Measurements and modeling of throughfall variability for five forest communities in the southeastern us. *Journal of Hydrology*, *312*(1-4), 95–108.

Calder, I. R. [I. R.]. (1990). Evaporation in the uplands. *Evaporation in the uplands*. doi:10.1016/0378-3774(91)90039-L

Calder, I. R. [Ian R]. (2001). Canopy processes: Implications for transpiration, interception and splash induced erosion, ultimately for forest management and water resources. In *Tropical forest canopies: Ecology and management* (pp. 203–214). Springer.

Cardellach, E., Fabra, F., Rius, A., Pettinato, S., & D’Addio, S. (2012). Characterization of dry-snow sub-structure using GNSS reflected signals. *Remote Sensing of Environment*, *124*(124), 122–134. doi:10.1016/j.rse.2012.05.012

Carlyle-Moses, D. E., & Price, A. G. (2007). Modelling canopy interception loss from a Madrean pine-oak stand, northeastern Mexico. *Hydrological Processes*, *21*(19), 2572–2580. doi:10.1002/HYP.6790

Carlyle-Moses, D., & Gash, J. [J.H.C.]. (2011). Rainfall interception loss by forest canopies. in: Forest hydrology and biogeochemistry: Synthesis of past research and future directions. Springer.

Chang, X., Jin, T., Yu, K., Li, Y., Li, J., & Zhang, Q. (2019). Soil moisture estimation by gnss multipath signal. *Remote Sensing*, *11*(21), 2559. doi:10.3390/rs11212559

Chew. (n.d.). Soil moisture remote sensing using gps-interferometric reflectometry. Retrieved from https://scholar.colorado.edu/concern/graduate_thesis_or_dissertations/12579s30p

Chow, V. (1959). Handbook of applied hydrology. *New York: Mc Graw Hilld*.

Cisneros Vaca, C., Van Der Tol, C., & Ghimire, C. P. (2018). The influence of long-term changes in canopy structure on rainfall interception loss: A case study in Speulderbos, the Netherlands. *Hydrology and Earth System Sciences*, *22*(7), 3701–3719. doi:10.5194/HESS-22-3701-2018

David, T., Gash, J., Valente, F., Pereira, J., Ferreira, M., & David, J. (2006). Rainfall interception by an isolated evergreen oak tree in a mediterranean savannah. *Hydrological Processes: An International Journal*, *20*(13), 2713–2726.

Dawoud, S. (2012). GNSS principles and comparison, 1–10. Retrieved from https://www.snet.tu-berlin.de/fileadmin/fg220/courses/WS1112/snet-project/gnss-principles-and-comparison_dawoud.pdf%20(Accessed%20on%202%20February%202018)

De Jong, K., Goode, M., Liu, X., & Stone, M. (2014). Precise GNSS Positioning in Arctic Regions. *Society of Petroleum Engineers - Arctic Technology Conference 2014*, 857–866. doi:10.4043/24651-MS

Della Vecchia, A., Ferrazzoli, P., Wigneron, J.-P., & Grant, J. P. (2007). Modeling forest emissivity at l-band and a comparison with multitemporal measurements. *IEEE Geoscience and Remote Sensing Letters*, *4*(4), 508–512. doi:10.1109/LGRS.2007.900687

Della Vecchia, A., Saleh, K., Ferrazzoli, P., Guerriero, L., & Wigneron, J.-P. (2006). Simulating l-band emission of coniferous forests using a discrete model and a detailed geometrical representation. *IEEE Geoscience and Remote Sensing Letters*, *3*(3), 364–368. doi:10.1109/LGRS.2006.873230

Department Of Defense, U. (2008). Global Positioning System Standard Positioning Service. *Www.Gps.Gov*, (September), 1–160. Retrieved from http://www.gps.gov/technical/ps/2008-SPS-performance-standard.pdf

Dunne, T., & Leopold, L. B. (1978). *Water in environmental planning*. Macmillan.

Elosegui, P., Davis, J. L., Jaldehag, R. T., Johansson, J. M., Niell, A. E., & Shapiro, I. I. (1995). Geodesy using the Global Positioning System: The effects of signal scattering on estimates of site position. *Journal of Geophysical Research: Solid Earth*, *100*(B6), 9921–9934. doi:10.1029/95JB00868

Entekhabi, D., Njoku, E., & O'Neill, P. (2009). The soil moisture active and passive mission (smap): Science and applications. In *2009 ieee radar conference* (pp. 1–3). doi:10.1109/RADAR.2009.4977030

European Space Acency. (2018). GNSS Basic Observables. Retrieved May 17, 2022, from https://gssc.esa.int/navipedia/index.php/GNSS_Basic_Observables

Farzaneh, S., Parvazi, K., & Shali, H. H. (2021). GNSS-IR-UT: A MATLAB-based software for SNR-based GNSS interferometric reflectometry (GNSS-IR) analysis. *Earth Science Informatics*, *14*(3), 1633–1645. doi:10.1007/S12145-021-00637-Y/FIGURES/13

Gash, J. H. (1979). An analytical model of rainfall interception by forests. *Quarterly Journal of the Royal Meteorological Society*, *105*(443), 43–55. doi:10.1002/QJ.49710544304

Gash, J. H., Lloyd, C. R., & Lachaud, G. (1995). Estimating sparse forest rainfall interception with an analytical model. *Journal of Hydrology*, *170*(1-4), 79–86. doi:10.1016/0022-1694(95)02697-N

Gash, J. H., Wright, I. R., & Lloyd, C. R. (1980). Comparative estimates of interception loss from three coniferous forests in Great Britain. *Journal of Hydrology*, *48*(1-2), 89–105. doi:10.1016/0022-1694(80)90068-2

Gash, J. [JHC], & Morton, A. (1978). An application of the rutter model to the estimation of the interception loss from thetford forest. *Journal of hydrology*, *38*(1-2), 49–58.

Gernot, C. (2007). GPS Signal Disturbances by Water in Various States, 25–28.

Ghimire, C. P., Bruijnzeel, L. A., Lubczynski, M. W., & Bonell, M. (2012). Rainfall interception by natural and planted forests in the middle mountains of central nepal. *Journal of Hydrology*, *475*, 270–280.

Gómez, J., Giráldez, J., & Fereres, E. (2001). Rainfall interception by olive trees in relation to leaf area. *Agricultural water management*, *49*(1), 65–76.

Grant, J. P. [J. P.], Wigneron, J. P., Van de Griend, A. A., Kruszewski, A., Søbjærg, S. S., & Skou, N. (2007). A field experiment on microwave forest radiometry: L-band signal behaviour for varying conditions of surface wetness. *Remote Sensing of Environment*, *109*(1), 10–19. doi:10.1016/J.RSE.2006.12.001

Grant, J. P. [Jennifer P.], Saleh-Contell, K., Wigneron, J.-P., Guglielmetti, M., Kerr, Y. H., Schwank, M., … Van de Griend, A. A. (2008). Calibration of the l-meb model over a coniferous and a deciduous forest. *IEEE Transactions on Geoscience and Remote Sensing*, *46*(3), 808–818. doi:10.1109/TGRS.2007.914801

Guerriero, L., Martín, F., Mollfulleda, A., Paloscia, S., Pierdicca, N., Santi, E., & Floury, N. (2020). Ground-based remote sensing of forests exploiting gnss signals. *IEEE Transactions on Geoscience and Remote Sensing*, *58*(10), 6844–6860. doi:10.1109/TGRS.2020.2976899

Hafidhi, M. M., & Boutillon, E. (2016). Improving the performance of the carrier tracking loop for gps receivers in presence of transient errors due to pvt variations. In *2016 ieee international workshop on signal processing systems (sips)* (pp. 80–85). doi:10.1109/SiPS.2016.22

Hahirwabasenga, J. (2019). Estimating rainfall interception loss using sentinel-2 in the veluwe area, the netherlands. Retrieved from http://essay.utwente.nl/83351/

Hiemstra, P., & Sluiter, R. (2011). Interpolation of Makkink Evaporation in the Netherlands. *De Bilt, 2011 | Technical report; TR-327*, 78. Retrieved from https://cdn.knmi.nl/knmi/pdf/bibliotheek/knmipubTR/TR327.pdf

Hofmann-Wellenhof, B., Lichtenegger, H., & Collins, J. (2001). Global Positioning System: Theory and Practice, 1–10. doi:10.1007/978-3-7091-6199-9

Hofmann-Wellenhof, B., Lichtenegger, H., & Wasle, E. (2008). *Gnss – global navigation satellite systems gps, glonass, galileo, and more*. ISBN: 978-3-211-73012-6. Springer Vienna.

J. Sanz Subirana, J.M. Juan Zornoza and M. Hernández-Pajares, Technical University of Catalonia, Spain. (2011). Tropospheric Delay. Retrieved July 29, 2022, from https://gssc.esa.int/navipedia/index.php/Tropospheric_Delay

Jetten, V. (1996). Interception of tropical rain forest: Performance of a canopy water balance model. *Hydrological processes*, *10*(5), 671–685.

Jetten, V. G. [Victor Gerlof] et al. (1994). *Modelling the effects of logging on the water balance of a tropical rain forest: A study in guyana.*

Jiang, Z., & Groves, P. D. (2012). Nlos gps signal detection using a dual-polarisation antenna. *GPS Solutions*, *18*(1), 15–26. doi:10.1007/s10291-012-0305-5

Jin, S., Cardellach, E., & Xie, F. (2014). *GNSS Remote Sensing*. doi:10.1007/978-94-007-7482-7

Jin, S., & Komjathy, A. (2010). GNSS reflectometry and remote sensing: New objectives and results. *Advances in Space Research*, *46*(2), 111–117. doi:10.1016/j.asr.2010.01.014

Kaplan, E., & Hegarty, C. (2006). Understanding GPS. *Artech House*, 723. Retrieved from http://tocs.ulb.tu-darmstadt.de/135793181.pdf

Klaassen, W., Bosveld, F., & de Water, E. (1998). Water storage and evaporation as constituents of rainfall interception. *Journal of Hydrology*, *212-213*, 36–50. doi:10.1016/s0022-1694(98)00200-5

Komjathy, A., Armatys, M., Masters, D., Axelrad, P., Zavorotny, V., & Katzberg, S. (2004). Retrieval of ocean surface wind speed and wind direction using reflected gps signals. *Journal of Atmospheric and Oceanic Technology*, *21*(3), 515–526. doi:10.1175/1520-0426(2004)021<0515:rooSWS>2.0.co;2

Komjathy, A., Maslanik, J., Zavorotny, V. U., Axelrad, P., & Katzberg, S. J. (2000). Sea ice remote sensing using surface reflected GPS signals. *International Geoscience and Remote Sensing Symposium (IGARSS)*, *7*, 2855–2857. doi:10.1109/IGARSS.2000.860270

Kurum, M., O'Neill, P. E., Lang, R. H., Joseph, A. T., Cosh, M. H., & Jackson, T. J. (2012). Effective tree scattering and opacity at L-band. *Remote Sensing of Environment*, *118*, 1–9. doi:10.1016/J.RSE.2011.10.024

Larson, K. M. [Kristine M], Braun, J. J., Small, E. E., Zavorotny, V. U., Gutmann, E. D., & Bilich, A. L. (2009). Gps multipath and its relation to near-surface soil moisture content. *IEEE Journal of Selected Topics in Applied Earth Observations and Remote Sensing*, *3*(1), 91–99.

Larson, K. M. [Kristine M.], Löfgren, J. S., & Haas, R. (2013). Coastal sea level measurements using a single geodetic GPS receiver. *Advances in Space Research*, *51*(8), 1301–1310. doi:10.1016/J.ASR.2012.04.017

Larson, K. M. [Kristine M.], & Nievinski, F. G. (2013). GPS snow sensing: Results from the EarthScope Plate Boundary Observatory. *GPS Solutions*, *17*(1), 41–52. doi:10.1007/S10291-012-0259-7/FIGURES/11

Larson, K. M. [Kristine M.], Small, E. E., Gutmann, E., Bilich, A., Axelrad, P., & Braun, J. (2008). Using GPS multipath to measure soil moisture fluctuations: initial results. *GPS Solutions*, *12*(3), 173–177. doi:10.1007/s10291-007-0076-6

Liu, J., Hyyppa, J., Yu, X., Jaakkola, A., Kukko, A., Kaartinen, H., … Hyyppa, H. (2017). A Novel GNSS Technique for Predicting Boreal Forest Attributes at Low Cost. *IEEE Transactions on Geoscience and Remote Sensing*, *55*(9), 4855–4867. doi:10.1109/TGRS.2017.2650944

Llorens, P., & Domingo, F. (2007). Rainfall partitioning by vegetation under Mediterranean conditions. A review of studies in Europe. *Journal of Hydrology*, *335*(1-2), 37–54. doi:10.1016/J.JHYDROL.2006.10.032

Lowe, S. T., Zuffada, C., Chao, Y., Kroger, P., Young, L. E., & Labrecque, J. L. (2002). 5-cm-precision aircraft ocean altimetry using GPS reflections. *Geophysical Research Letters*, *29*(10), 13–1. doi:10.1029/2002gl014759

Ma, C., Li, X., Luo, Y., Shao, M., & Jia, X. (2019). The modelling of rainfall interception in growing and dormant seasons for a pine plantation and a black locust plantation in semi-arid Northwest China. *Journal of Hydrology*, *577*, 123849. doi:10.1016/J.JHYDROL.2019.06.021

Macgougan, G., Lachapelle, G., Nayak, R., & Wang, A. (2001). OVERVIEW OF GNSS SIGNAL DEGRADATION PHENOMENA, 87–100. Retrieved from http://plan.geomatics.ucalgary.ca/papers/macgougan_et_al_kis2001.pdf

Martín, A., Ibáñez, S., Baixauli, C., Blanc, S., & Anquela, A. B. (2020). Multi-constellation GNSS interferometric reflectometry with mass-market sensors as a solution for soil moisture monitoring. *Hydrology and Earth System Sciences*, *24*(7), 3573–3582. doi:10.5194/hess-24-3573-2020

Martin-Neira, M. (1993). A passive reflectometry and interferometry system (PARIS): application to ocean altimetry. *ESA Journal*, *17*(4), 331–355.

Masters, D. S. (2004). Surface remote sensing applications of GNSS bistatic radar: Soil moisture and aircraft altimetry. *ProQuest Dissertations and Theses*, *3153856*, 224–224. Retrieved from http://ezproxy.net.ucf.edu/login?url=http://search.proquest.com/docview/305203577?accountid=10003%5Cnhttp://sfx.fcla.edu/ucf?url_ver=Z39.88-2004&rft_val_fmt=info:ofi/fmt:kev:mtx:dissertation&genre=dissertations+&+theses&sid=ProQ:ProQuest+Dissertations+&+T

Mateos, B., & Schnabel, S. (2001). Rainfall interception by holm oaks in mediterranean open woodland. *Cuadernos de Investigación Geográfica*, *27*, 27–38.

McCreight, J. L., Small, E. E., & Larson, K. M. (2014). Snow depth, density, and SWE estimates derived from GPS reflection data: Validation in the western U. S. *Water Resources Research*, *50*(8), 6892–6909. doi:10.1002/2014WR015561

Muzylo, A., Llorens, P., Valente, F., Keizer, J. J., Domingo, F., & Gash, J. H. (2009). A review of rainfall interception modelling. *Journal of Hydrology*, *370*(1-4), 191–206. doi:10.1016/J.JHYDROL.2009.02.058

Nadkarni, N. M., Merwin, M. C., & Nieder, J. (2013). Forest canopies, plant diversity. *Encyclopedia of Biodiversity*, 516–527. doi:10.1016/b978-0-12-384719-5.00158-1

National Aeronautics and Space Administration, Science Mission Directorate. (2010). Waves Behaviours. Retrieved May 17, 2022, from https://science.nasa.gov/ems/03_behaviors

O'Driscoll, C. (2010). GNSS Solutions: Carrier phase and its measurement for GNSS. *Inside GNSS*, (July/August 2010), 18–22. Retrieved from www.insidegnss.com%20http://scholar.google.com/scholar?hl=en&btnG=Search&q=intitle:GNSS+Solutions+:#0

Oliveira, L. B., Zapella, M., & Hunt, R. (2018). Global Positioning System and GLObal NAvigation Satellite System constellations for better time synchronising reliability. *The Journal of Engineering*, *2018*(15), 935–937. doi:10.1049/JOE.2018.0183

Oxley, A. (2017). Sources of Inaccuracy. *Uncertainties in GPS Positioning*, 99–114. doi:10.1016/B978-0-12-809594-2.00008-3

Parker, G. G., Lowman, M. D., & Nadkarni, N. M. (1995). Structure and microclimate of forest canopies.

Patenaude, G., Milne, R., & Dawson, T. P. (2005). Synthesis of remote sensing approaches for forest carbon estimation: reporting to the Kyoto Protocol. doi:10.1016/j.envsci.2004.12.010

Pereira, F., Gash, J., David, J., David, T., Monteiro, P., & Valente, F. (2009). Modelling interception loss from evergreen oak mediterranean savannas: Application of a tree-based modelling approach. *Agricultural and Forest Meteorology*, *149*(3-4), 680–688.

Perez-Ruiz, M., & K., S. (2012). GNSS in Precision Agricultural Operations. *New Approach of Indoor and Outdoor Localization Systems*. doi:10.5772/50448

Peter J.G. Teunissen, & Oliver Montenbruck. (2017). Springer Handbook of Global Navigation Satellite Systems. *Springer Handbook of Global Navigation Satellite Systems*. doi:10.1007/978-3-319-42928-1

Pypker, T. G., Bond, B. J., Link, T. E., Marks, D., & Unsworth, M. H. (2005). The importance of canopy structure in controlling the interception loss of rainfall: Examples from a young and an old-growth douglas-fir forest. *Agricultural and Forest Meteorology*, *130*(1-2), 113–129. doi:10.1016/j.agrformet.2005.03.003

Raj, R., Alexander Samuel Hamm, N., Van Der Tol, C., & Stein, A. (2016). Uncertainty analysis of gross primary production partitioned from net ecosystem exchange measurements. *Biogeosciences*, *13*(5), 1409–1422. doi:10.5194/bg-13-1409-2016

Rodriguez-Alvarez, N., Bosch-Lluis, X., Camps, A., Aguasca, A., Vall-llossera, M., Valencia, E., … Park, H. (2011). Review of crop growth and soil moisture monitoring from a ground-based instrument implementing the Interference Pattern GNSS-R Technique. *Radio Science*, *46*(6). doi:10.1029/2011RS004680

Rodriguez-Alvarez, N., Bosch-Lluis, X., Camps, A., Ramos-Perez, I., Valencia, E., Park, H., & Vall-llossera, M. (2012). Vegetation water content estimation using gnss measurements. *IEEE Geoscience and Remote Sensing Letters*, *9*(2), 282–286. doi:10.1109/LGRS.2011.2166242

Rodriguez-Alvarez, N., Camps, A., Vall-llossera, M., Bosch-Lluis, X., Monerris, A., Ramos-Perez, I., … Sanchez, N. (2011). Land Geophysical Parameters Retrieval Using the Interference Pattern GNSS-R Technique. *IEEE Transactions on Geoscience and Remote Sensing*, *49*(1), 71–84. doi:10.1109/TGRS.2010.2049023

Roesler, C., & Larson, K. M. [Kristine M.]. (2018). Software tools for GNSS interferometric reflectometry (GNSS-IR). *GPS Solutions*, *22*(3), 1–10. doi:10.1007/s10291-018-0744-8

Rotenberg, E., & Yakir, D. (2010). Contribution of semi-arid forests to the climate system. *Science*, *327*(5964), 451–454.

Rutter, A. J., Morton, A. J., & Robins, P. C. (1975). A Predictive Model of Rainfall Interception in Forests. II. Generalization of the Model and Comparison with Observations in Some Coniferous and Hardwood Stands. *The Journal of Applied Ecology*, *12*(1), 367. doi:10.2307/2401739

Small, E. E., Larson, K. M., & Braun, J. J. (2010). Sensing vegetation growth with reflected GPS signals. *Geophys. Res. Lett*, *37*, 12401. doi:10.1029/2010GL042951

Soubie, R., Heinesch, B., Granier, A., Aubinet, M., & Vincke, C. (2016). Evapotranspiration assessment of a mixed temperate forest by four methods: Eddy covariance, soil water budget, analytical and model. *Agricultural and Forest Meteorology*, *228-229*, 191–204. doi:10.1016/j.agrformet.2016.07.001

Speulderbos. (n.d.). https://forestgeo.si.edu/sites/europe/speulderbos. Accessed: 2022-06-21.

Swaszek, P. F., Hartnett, R. J., Seals, K. C., Siciliano, J. D., & Swaszek, R. M. (2018). Limits on GNSS performance at high latitudes. In *Proceedings of the 2018 international technical meeting of the institute of navigation, itm 2018* (Vol. 2018-Janua, pp. 160–176). doi:10.33012/2018.15549

Takasu, T. (2013). RTKLIB ver. 2.4.2 Manual. Retrieved from https://www.rtklib.com/prog/manual_2.4.2.pdf

Tsiko, C. T., Makurira, H., Gerrits, A. M., & Savenije, H. H. (2012). Measuring forest floor and canopy interception in a savannah ecosystem. doi:10.1016/j.pce.2011.06.009

Vu, P. L. (2019). *Spatial altimetry, GNSS reflectometry and marine surcotes* (PhD dissertation, Université Toulouse III - Paul Sabatier). Retrieved from https://tel.archives-ouvertes.fr/tel-02896371

Wang, X., Zhang, Q., & Zhang, S. (2018). Water levels measured with SNR using wavelet decomposition and Lomb–Scargle periodogram. *GPS Solutions*, *22*(1), 1–10. doi:10.1007/s10291-017-0684-8

Ward, N. (1997). Understanding gps — principles and applications. elliott d. kaplan (editor). £75. isbn: 0-89006-793-7. artech house publishers, boston amp; london. 1996. *Journal of Navigation*, *50*(1), 151–152. doi:10.1017/S0373463300023730

Warner, J. S., & Johnston, R. G. (2003). Gps spoofing countermeasures.

Wright, W. C., Liu, P. W., Slatton, K., Shrestha, R. L., Carter, W., & Lee, H. (2008). Predicting l-band microwave attenuation through forest canopy using directional structuring elements and airborne lidar. In *Igarss 2008 - 2008 ieee international geoscience and remote sensing symposium* (Vol. 3, pp. III - 688-III –691). doi:10.1109/IGARSS.2008.4779441

Zavorotny, V. U., Gleason, S., Cardellach, E., & Camps, A. (2014). Tutorial on remote sensing using GNSS bistatic radar of opportunity. *IEEE Geoscience and Remote Sensing Magazine*, *2*(4), 8–45. doi:10.1109/MGRS.2014.2374220